HIPPOCAMPUS 19:1159–1186 (2009)

Cortical Efferents of the Perirhinal, Postrhinal, and Entorhinal Cortices of the Rat

Kara L. Agster[1] and Rebecca D. Burwell[1,2*]

ABSTRACT: We investigated the cortical efferents of the parahippocampal region by placing injections of the anterograde tracers, *Phaseolus vulgaris*-leuccoagglutinin, and biotinylated dextran amine, throughout the perirhinal (PER), postrhinal (POR), and entorhinal cortices of the rat brain. The resulting density of labeled fibers was evaluated in 25 subregions of the piriform, frontal, insular, temporal, cingulate, parietal, and occipital areas. The locations of labeled terminal fibers differed substantially depending on whether the location of the injection site was in PER area 35, PER area 36, POR, or the lateral or the medial entorhinal (LEA and MEA). The differences were greater for sensory regions. For example, the POR efferents preferentially target visual and spatial regions, whereas the PER efferents target all sensory modalities. The cortical efferents of each region largely reciprocate the cortical afferents, though the degree of reciprocity varied across originating and target regions. The laminar pattern of terminal fibers was consistent with the notion that the efferents are feedback projections. The density and amount of labeled fibers also differed substantially depending on the regional location of injection sites. PER area 36 and POR give rise to a greater number of heavy projections, followed by PER area 35. LEA also gives rise to widespread cortical efferents, arising mainly from a narrow band of cortex adjacent to the PER. In contrast, the remainder of the LEA and the MEA provides only weak efferents to cortical regions. Prior work has shown that nonspatial and spatial information is transmitted to the hippocampus via the PER-LEA and POR-MEA pathways, respectively. Our findings suggest that the return projections follow the same pathways, though perhaps with less segregration. © **2009 Wiley-Liss, Inc.**

KEY WORDS: hippocampus; memory; spatial; object

INTRODUCTION

Recent research has highlighted the importance of the parahippocampal region in various aspects of learning and memory, but the specific roles of these regions have not been precisely described. Available evidence suggests that the entorhinal cortex (EC) contributes to spatial navigation (Fyhn et al., 2004; Hafting et al., 2005; Lipton et al., 2007) and working memory (Egorov et al., 2002; Jarrard et al., 2004; McGaughy et al., 2005). The perirhinal cortex (PER) is known to be involved in object recognition (Wiig et al., 1996; Ennaceur and Aggleton, 1997; Eacott and Gaffan, 2005; Winters and Bussey, 2005b), discrimination learning (Young et al., 1997; Eacott et al., 2003; Campolattaro and Freeman, 2006a,b), perception (Bussey et al., 2003), and contextual learning (Bucci et al., 2000, 2002; Burwell et al., 2004b). The rat postrhinal cortex (POR), the structural homolog of the primate parahippocampal cortex, contributes to learning about context and object location (Malkova and Mishkin, 2003; Burwell et al., 2004a; Norman and Eacott, 2005). In addition, the PER and POR appear to play a role in conditioned orienting to visual stimuli (Bucci and Burwell, 2004). The evidence for such varied functions in medial temporal lobe structures highlights the importance of understanding how the different structures interact with each other, as well as other cortical structures.

Prior studies have examined various aspects of the cortical connectivity of the parahippocampal region. The cortical afferents of the PER have been described in rat (Deacon et al., 1983; Room and Groenewegen, 1986; Burwell and Amaral, 1998a). McIntyre et al. (1996) examined the cortical efferents; however, that study examined only the efferents of the anterior PER

[1] **Department of Neuroscience, Brown University, Providence, Rhode Island;** [2] **Department of Psychology, Brown University, Providence, Rhode Island**

Grant sponsor: NSF; Grant number: IBN9875792; Grant sponsor: NRSA; Grant number: NIH MH072144.

Abbreviations used: Area 35, 35 area 35 of the perirhinal cortex; ACAd, dorsal anterior cingulate area; ACAv, ventral anterior cingulate area; AId, dorsal agranular insular area; AIp, posterior agranular insular area; AIv, ventral agranular insular area; Area 36, 36 area 36 of the perirhinal cortex; AUD, primary auditory area; AUDp, posterior auditory area; AUDv, ventral auditory area; BDA, biotinylated dextran amine; CA1, CA2, CA3, CA, fields of the hippocampus; DAB, diaminobenzidine; DG, dentate gyrus; EC, entorhinal cortex; GU, gustatory area; ILA, infralimbic area; KPBS, potassium phosphate buffered saline; LEA, lateral entorhinal area; MEA, medial entorhinal area; Mop, primary motor area; MOs, secondary motor areas; NGS, normal goat serum; ORBl, lateral orbital area; ORBm, medial orbital area; ORBv, ventral orbital area; ORBvl, ventrolateral orbital area; PAP, peroxidase-antiperoxidase; PBS, phosphate-buffered saline; PER, perirhinal cortex; PHA-L, Phaseolus vulgaris-leuccoagglutinin; PIR, piriform cortex; PL, prelimbic area; POR, postrhinal cortex; PTLp, posterior parietal association areas; rs, rhinal sulcus; RSPd, dorsal retrosplenial area; RSPv, ventral retrosplenial area; SSp, primary somatosensory area; SSs, supplementary somatosensory area; TEv, ventral temporal association areas; VISC, visceral area; VISl, lateral visual areas; VISm, medial visual areas; VISp, primary visual area.

Kara L. Agster is currently at Department of Neurobiology and Anatomy, Drexel University College of Medicine, Philadelphia, PA, USA.

*Correspondence to: Rebecca D. Burwell, Department of Psychology, Brown University, Providence, RI 02912, USA. E-mail: Rebecca_Burwell@Brown.edu

Accepted for publication 16 January 2009
DOI 10.1002/hipo.20578
Published online 9 April 2009 in Wiley InterScience (www.interscience.wiley.com).

and did not attempt to differentiate the efferents of area 35 from those of area 36. Other studies have addressed efferents and afferents, but only for a single region, for example the EC (Van Hoesen et al., 1972; Witter and Groenewegen, 1986; Insausti et al., 1987). Such studies do not permit direct comparisons of the strength and topography of connections across regions. Comparisons across regions are also hampered by differences in the borders, regions, and methods used in the available studies.

The aim of this study was to characterize the cortical efferents of the rat PER areas 35 and 36, the POR, and entorhinal areas LEA and MEA such that the relative strength of cortical efferents as well as reciprocity could be assessed. We quantified labeled fibers in 26 cortical regions following tract tracer injections in these five areas. Some preliminary findings of this study were previously summarized in commentaries (Furtak et al., 2007; Kerr et al., 2007), but are presented here in complete detail. Data obtained from this study complement our prior work on the cortical afferents of the same regions using the same borders (Burwell and Amaral, 1998a). With these new data, we now have a complete picture of the cortical connectivity of PER areas 35 and 36, POR, and the LEA and MEA of the rat brain.

NOMENCLATURE

The borders and histological criteria for the POR and the PER areas 35 and 36 (Fig. 1A) are according to Burwell (2001). Briefly, PER cortex is located near the rhinal fissure, caudal to insular cortex, and dorsal to the lateral entorhinal area (LEA). The region is subdivided into the dorsally situated area 36 and the ventrally situated area 35. The POR forms the caudal border of the PER cortex and lies dorsal to the medial entorhinal area (MEA). For the EC, we relied on the cytoarchitectonic descriptions of Insausti et al. (1997). That definition includes six subdivisions. For this study, however, the four rostral and lateral subdivisions were combined to form the LEA and the two caudal and medial regions were combined to form the MEA following Dolorfo and Amaral (1998a).

The EC in rats and monkeys is organized into multiple bands that project to different septotemporal levels of the dentate gyrus (DG) (Witter, 1989; Witter et al., 1989b; Dolorfo and Amaral, 1998a,b). Dolorfo and Amaral (1998a,b) showed that the EC is organized into three bands that project to different septotemporal levels of the dentate gyrus (DG, Fig. 1B). Each of the three bands spans both the LEA and MEA. Projections originating in the lateral band of the EC terminate preferentially in the dorsal half of the DG. Projections arising from the intermediate and medial bands of the EC terminate in the third and fourth quarters of the DG, respectively. The intrinsic connections of the DG-projecting bands terminate in the band of origin. Thus, the LEA and MEA are heavily interconnected within a band. The anatomical organization suggests that the bands may be functionally distinct. For that reason, we have

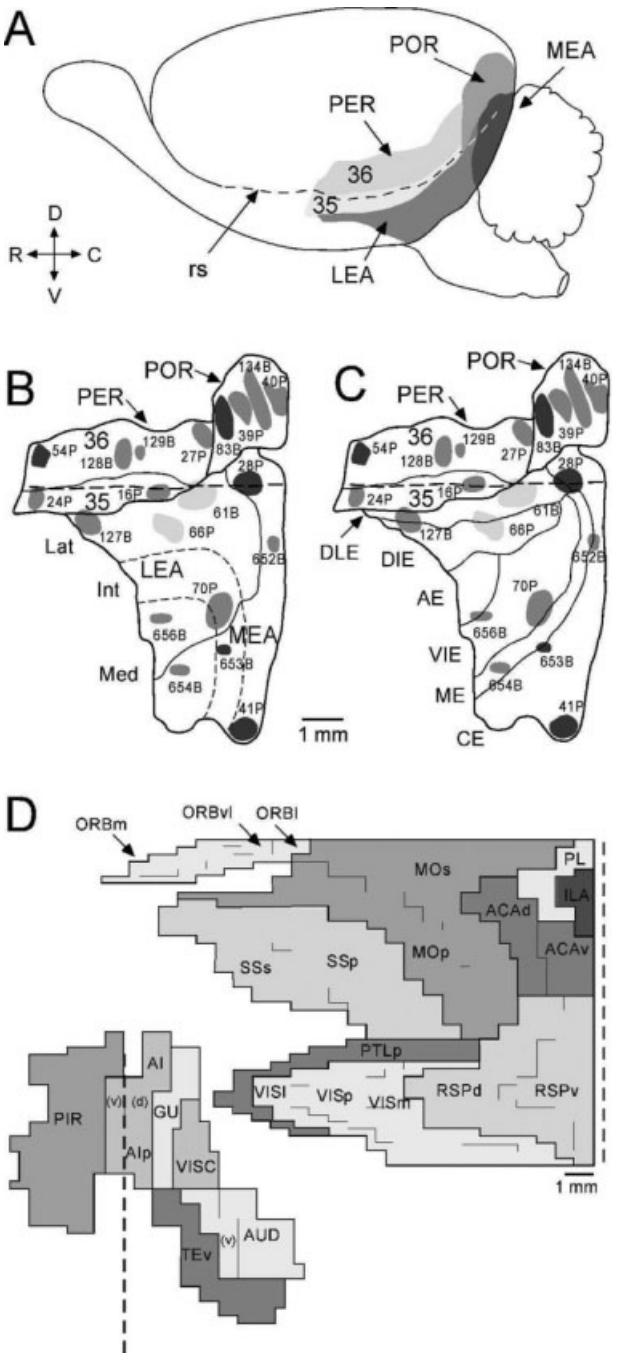

FIGURE 1. Schematics of the perirhinal (PER), postrhinal (POR), and entorhinal (EC) cortices. (A) Lateral surface view of the rat brain showing the location of PER areas 35 and 36, POR, and entorhinal areas LEA and MEA. (B) Location of the anterograde tracer injection sites according to region and DG-projecting bands. Dark gray and light gray indicate tracer injections in deep and superficial layers of cortex. Medium gray indicates tracer injections that spanned superficial and deep layers of cortex. Injection sites are labeled with the names of respective cases (Table 1). (C) Location of injection sites according to the entorhinal parcellation by Insausti et al. (1997). (D) Schematic of a generic unfolded map of the target regions showing subdivisions. Note that PTLp has two limbs, which we term the dorsal and caudal limbs. B, biotinylated dextrane; C, caudal; D, dorsal; P, PHA-L; R, rostral; V, ventral. See list for other abbreviations. Scale bar: 1 mm.

also addressed the cortical efferents with respect to these intrinsic bands of connectivity. The location of each injection site in the EC was identified with respect to subregion (LEA or MEA) based on the local cytoarchitectonic features and with respect to the finer parcellation of Insausti et al. (1997). Sites were further characterized as belonging to one of the dentate-projecting bands by referencing material to coronal sections shown by Dolorfo and Amaral (1998a,b).

Density of labeled fibers was assessed in seven cortical areas comprising 26 subdivisions (Fig. 1D). We previously described the criteria used to demarcate cortical targets of the PER, POR, and the EC (Burwell and Amaral, 1998a). Here, we briefly describe the criteria and provide appropriate references. Unless specified, we relied on commonly used stereotaxic rat brain atlases for boundaries and nomenclature (e.g., Swanson, 1992; Paxinos and Watson, 1998).

Boundaries and cytoarchitecture of the piriform area (PIR) are well-described (Rose, 1929; Krieg, 1946; Haberly and Price, 1978). For this study, we relied more heavily on the boundaries and nomenclature as presented by Swanson (1992).

Seven regions in frontal cortex were examined (Fig. 1D). These included the primary and supplementary motor areas (MOp and MOs), prelimbic area (PL), infralimbic area (ILA), and the medial, lateral, and ventrolateral orbitofrontal regions (ORBm, ORBl, and ORBvl, respectively). Borders and cytoarchitectonic features of MOp and MOs followed those described by Donoghue and Wise (1982). Boundaries and nomenclature for the remaining frontal regions were according to Krettek and Price (1977). Note that PL and infralimbic cortices could also be included in the cingulate regions (Jones and Witter, 2007). We have included them with the frontal regions to be consistent with the companion study (Burwell and Amaral, 1998a).

Insular cortex was divided into dorsal, ventral, and posterior agranular insular regions (AId, AIv, and AIp, respectively, Fig. 1D) (Krettek and Price, 1977). In addition, two granular areas, the gustatory (GU) and visceral (VISC) cortices, were examined. Nomenclature and boundaries for these regions are taken from (Swanson, 1992).

The ventral temporal region (TEv) is defined according to Swanson (1992). This region is further defined as a strip of cortex dorsally adjacent to the PER region described by Burwell (2001). Temporal regions also included auditory cortex (Fig. 1D). Primary and dorsal auditory areas defined by Swanson (1992) were combined and are referred to by the abbreviation AUD (Mascagni et al., 1993). A ventral supplementary or belt region (AUDv) was investigated separately because it is considered unimodal sensory association cortex (Arnault and Roger, 1990).

Borders and features of primary and supplementary somatosensory regions (SSp and SSs, Fig. 1D) were taken from Chapin and Lin (1984). The posterior parietal region was first defined by (Krieg, 1946). The borders were redefined by Swanson (1992) and termed PTLp. The region is a long strip of cortex with two limbs. The dorsal limb extends laterally from near the midline and then turns caudally to form the caudal limb (Fig. 1D). It should be noted that the somatosensory regions could have been categorized differently. We have included them as a part of the parietal regions along with the posterior parietal cortex to be consistent with an earlier study (Burwell and Amaral, 1998a).

For the dorsal and ventral anterior cingulate (ACAd and ACAv) regions, we followed boundaries proposed by Krettek and Price (1977). Two other regions, the agranular retrosplenial area (RSPd) and granular retrosplenial area (RSPv) were also examined (Krettek and Price, 1977; Vogt and Miller, 1983).

The boundaries for the primary visual area (VISp) were taken from Swanson (1992). We also examined two visual association regions, a lateral and medial area (VISl and VISm). Criteria and borders for visual association regions were taken from Paxinos and Watson (1998).

MATERIALS AND METHODS

Subjects

Twenty-nine male Sprague-Dawley rats weighing between 300 and 400 g served as subjects. Data from 24 of those animals were previously analyzed to assess intrinsic connections of the PER, POR, and EC as reported in an earlier study (Burwell and Amaral, 1998a). Prior to surgery, subjects were housed individually or in pairs under standard 12 h light/12 h dark conditions with ad libitum access to food and water. Following surgery, all subjects were housed individually. All methods involving the use of live animals conformed to NIH guidelines and were approved by the appropriate Institutional Animal Care and Use Committee.

Tract Tracers, Reagents, and Antibodies

Two different anterograde tracers were used in these studies. The biotinylated dextran amine (BDA) used in these studies was obtained from Molecular Probes (Eugene, OR, now owned by Invitrogen, Corp.). We used the 10,000 MW biotinylated dextran conjugated to lysine (Catalog No. D1956). BDA was visualized with an avidin-biotinylated horseradish peroxidase procedure (Super ABC Kit; Biomeda Corporation) followed by a metal-enhanced diaminobenzidine (DAB) reaction. Veenman et al. (1992) demonstrated that iontophoretic injections of BDA in cortex using these visualization techniques lead to extensive anterograde fiber labeling of axons and terminals in forebrain after 1 week survival time.

The *Phaseolus vulgaris*-leuccoagglutinin (PHA-L) used in these studies was obtained from Vector Laboratories, Burlingame, CA. (Catalog No. B-1,115). PHA-L was found to be an excellent, specific marker for use as an anterograde neuronal tracer (Gerfen and Sawchenko, 1984). For PHA-L experiments, we either used a biotinylated secondary procedure or a peroxidase-antiperoxidase (PAP) procedure. The primary antibody was a rabbit anti-PHA-L antibody (B-275, Dako, Carpinteria,

CA). For the biotinylated procedure, the secondary antibody was biotinylated goat-antirabbit IgG (Vector, Catalog No. BA-1000). For the PAP procedures, the secondary antibody was a goat antirabbit IgG (Catalog No. 401, Sternberger Monoclonals, Baltimore, MD). The final antibody was the rabbit PAP (Catalog No. 503, Sternberger Monoclonals, Baltimore, MD).

Surgery

Surgical procedures were performed as previously reported (Burwell and Amaral, 1998a). Briefly, animals were anesthetized with sodium pentobarbital, halothane, or isoflurane and secured in a stereotaxic appartus (Kopf, Tujunga, CA). An incision was made in the skin over the skull and the connective tissue was retracted. Craniotomies were made in the skull overlying the intended injection sites. Coordinates of the intended cortical targets were adapted from Paxinos and Watson (1998).

Anterograde tracer injections of BDA or PHA-L were made in the EC ($n = 14$), PER ($n = 10$), or POR ($n = 5$) cortices. BDA was prepared in a 10% solution in 0.1 M phosphate buffered saline (PBS). PHA-L was prepared in a 2.5% solution in 0.1 M PBS. Tracers were injected via iontophoresis with positive DC current (4 μamps; 8 s on, 8 s off) for 8 min through glass micropipettes. Micropipettes had an average tip diameter of 4–5 μm. Following the injection procedure, the wound was sutured, and the animal was monitored for several hours. Upon demonstrating normal levels of activity, subjects were returned to the colony for a 7–14 day survival period.

Tissue Processing

Subjects were deeply anesthetized with an intraperitoneal injection of either chloral hydrate or Beuthanasia (Schering-Plough, Kenilworth, NJ) and transcardially perfused using a pH-shift protocol (Burwell and Amaral, 1998b). Solutions were perfused at a flow rate of 35–40 ml/min. Two minutes of room temperature saline was followed by 10 min of 4% paraformaldehyde in 0.1 M sodium acetate buffer (pH 6.5 at 4°C) and 15 min of 4% paraformaldehyde in 0.1 M sodium borate buffer (pH 9.5 at 4°C). Ice was packed around the subject's head during perfusion. Brains were removed from the skull, postfixed for 6 h in the paraformaldehyde/sodium borate solution at 4°C, and cryoprotected for 24 h in 20% glycerol in 0.02 M potassium PBS (KPBS, pH 7.4 at 4°C). The brains were then blocked and frozen. The brains were either immediately sectioned or stored at −80°C for later processing.

Each brain was cut into five series of 30 μm sections beginning at the rostral limit of prefrontal cortex and extending through the caudal pole of the neocortex. A single 1:5 series was mounted and stained for Nissl material with thionin. A second series was collected into 0.1 M KPBS for anterograde tracer processing. The remaining three series were used for other procedures or stored at −80°C in a cryoprotectant tissue collecting solution of 30% ethylene glycol and 20% glycerol in sodium phosphate buffer (for details, see Burwell and Amaral, 1998b).

An avidin-biotin reaction was used to visualize BDA labeled fibers. To facilitate penetration of reagents, sections were initially pretreated in a 1% solution of Triton X-100 in KPBS for 1 h. Sections were then incubated overnight at 4°C in a solution of avidin reagent and stabilizer (1:25 and 1:50 dilutions, respectively) in KPBS plus 0.1% solution of Triton X-100. After three 10 min washes in KPBS, sections were processed for visualization by incubation in 0.05% 3,3′-DAB (Pierce, Tacoma, WA) and 0.04% hydrogen peroxide in KPBS for 10–30 min.

PHA-L processing utilized one of two methods depending on whether there were one or two anterograde tract tracer injections in the brain (for details, see Burwell and Amaral, 1998b). When only one tracer was used, the procedure involved a biotinylated secondary antibody, with an avidin-biotin incubation (method adapted from Gerfen and Sawchenko, 1984). To minimize nonspecific binding, sections were initially incubated for 2–3 h in 5% normal goat serum (NGS) and 0.5% Triton-X 100 in KPBS. Sections were then incubated in the primary antiserum solution of rabbit anti-PHA-L (1:12,000 dilution) in 0.3% Triton-X 100 and 2% NGS in KPBS for 42–48 h. After two 10 min washes in 2% NGS in KPBS, sections were incubated in the biotinylated secondary antibody solution containing goat antirabbit IgG (1:277 dilution) in 0.3% Triton-X 100, and 2% NGS in KPBS for 45 min. Tissue sections were then washed twice in 2% NGS in KPBS and visualized by incubation in 0.05% DAB and 0.04% hydrogen peroxide in KPBS for 5–10 min. The second method employed a PAP complex rather than the avidin reagent. The procedure was the same as above except that the secondary antiserum was goat antirabbit IgG at a 1:200 dilution followed by a rabbit-PAP incubation.

Once all immunohistochemical processing was completed, sections were washed in KPBS, mounted on gelatin coated slides, dried, defatted, and intensified with osmium tetroxide and thiocarbohydrate or gold chloride.

Anatomical Analysis

Twenty-nine cases with injections located in POR, PER area 35, PER area 36, LEA, or MEA were reviewed for possible inclusion in the study, and 20 cases were selected for detailed analysis (Fig. 1C and Table 1). Cases selected were included to cover the extent of the regions of origin. Data obtained from PER areas 35 and 36 and from the LEA and MEA are presented individually. Labeled fibers arising from EC injection sites were also analyzed with respect to the band of origin. The location of the bands were estimated based on the analyses and descriptions reported in the earlier study by Dolorfo and Amaral (1998a,b). Labeled fibers were quantified for subregions within the piriform, frontal, insular, temporal, cingulate, parietal, and occipital cortices (see Nomenclature section and Fig. 2).

The data presented in this article were documented in multiple ways. To provide quantitative measures of anterograde material, we provided two average measures of density, one that

TABLE 1.

Anterograde Tracer Injection Sites

Location	Experiment	Layer	Surface area (sq. mm)
Perirhinal			
Rostral area 36	54P	V–VI	0.72
Mid-rostrocaudal area 36	128B	II–VI	0.54
Caudal area 36	27P	II–VI	0.45
Ventral area 36	129B	II–V	0.18
Rostral area 35	24P	III–VI	0.27
Caudal area 35	16P	II–V	0.27
Postrhinal			
Rostral	39P	I–VI	0.63
Rostrodorsal	83B	V–VI	0.45
Dorsal	134B	I–VI	0.99
Caudal	40P	III–VI	0.54
Entorhinal			
Rostral LEA (LB)	127B[a]	III–VI	0.90
Mid-rostrocaudal LEA (LB)	66P	II–III[b]	0.63
Caudal LEA (LB)	61B[c]	I–III[b]	0.63
Caudomedial LEA (IB)	70P	III–IV	0.99
Rostromedial LEA (MB)	656B	II–V	0.72
Lateral MEA (LB)	28P	V–VI	0.27
Ventral MEA (LB)	652B	II–IV	0.45
Medial MEA (LB)	41P	V–VI	0.36
Medial MEA (IB)	653B	II–VI	0.45
Rostromedial MEA (MB)	654B	III–VI	0.36

Anterograde injections sites are suffixed with a P or a B for PHA-L and BDA, respectively. Entorhinal lateral, intermediate, and medial bands are designated LB, IB, and MB, respectively.

[a]Experiment 127B encroached slightly on deep layers of area 35.

[b]Though the injection site was largely in superficial layers for Cases 61B and 66P, nearly one-third of the labeled cells were located in layers V and VI for both cases.

[c]Experiment 61B encroached slightly on superficial layers of area 36.

was normalized for volume (Table 2) and one that was not (Table 3). Using *camera lucida* methods and a voxel approach, we assessed the detailed locations of labeled fibers. These data were presented in the unfolded density maps. The unfolded maps, together with location of the tracer injections, permitted assessment of the point to point topography of connections. Photomicroscopy was used to document examples of the anatomical material and to illustrate verbal assessments of density and laminar location of labeled fibers. The aspects of the data that were most striking and were the most meaningful to research on learning and memory were highlighted in the results.

For quantification of the anterograde label, adjacent sections were stained for Nissl material and used to draw the outlines and borders of the individual cortical regions using camera lucida methods (Leica MZ6 stereomicroscope with brightfield and darkfield capability). Coronal sections were drawn for a 1:10 series of 30 μm sections (at 300 μm intervals). The midline border of anterior cingulate and retrosplenial regions served as a fixed reference point. In sections rostral to the anterior cingulate, prelimbic/infralimbic areas were used as the reference point. The outline of the cortical surface was then subdivided into 600 μm segments. Lines were drawn perpendicular from the pial surface to the deep border of layer VI to create a series of cortical columns. Drawings of coronal sections were aligned with the anterograde material for quantification of density of labeled fibers using dark field microscopy. The density of labeled fibers within a column was determined according to a rating scale of 0 to 6. A score of 0 indicated no fibers were present, whereas a score of 6 denoted heavy density of labeled fibers within the column. Criteria for scoring were developed on a case by case basis, such that the heaviest density of labeled fibers observed for that case would receive a score of 6. Adjacent parahippocampal regions were also sampled to develop the criteria, even though those regions were not analyzed in this study.

Only fibers that showed characteristics of terminal fibers were scored. Fibers that were thin, exhibited varicosities or boutons, and tended to ramify were considered to be innervating the location in which they appeared and were included in the density analysis. Labeled fibers that showed characteristics of en passant fibers were not scored. Unscored labeling included fibers that were large and smooth and that exhibited few ramifications and no terminal boutons.

For visualization of the density of labeled fibers, two-dimensional straight-line unfolded maps of the cerebral cortex were created for each case using a procedure we developed earlier (Burwell and Amaral, 1998b). Briefly, the density ratings for the cortical columns were entered into cells of a Microsoft Excel spreadsheet, beginning with a defined reference point. For the more dorsal regions, we used the ventral borders of the ACAv and RSPv as the reference point. We used the rhinal fissure for the more ventral regions. The location of the cortical borders was added. We developed macros to convert ratings of density of labeled fibers into a color scale. The unfolded maps were then converted to Canvas (Deneba Software, Miami, FL) for illustration purposes. For some areas, including visual and prefrontal regions, we did not include all boundaries because the resulting maps were difficult to parse visually. Instead, we provided a normalized template in Figure 1D that includes all areas.

Density scores were further analyzed in two ways to evaluate the differences in the density of labeled fibers resulting from tracer injections located in different parahippocampal regions. First, an average of the density ratings was computed for each of the 26 cytoarchitectonically defined cortical regions for each case. This provided an assessment of the average density of labeled fibers in each neocortical target region that was independent of the volume of the target region. This approach is useful for comparing the density of labeled fibers in the same target regions arising from different projection regions. As an example, this method permits a comparison of the overall strength of the PER area 36 and area 35 projections to PTLp. Average densities, however, may not be as useful for comparing the strength of projections across target regions that differ in volume. To explain, when the measure is average density, moderately heavy fiber labeling in a large region receives the same rating as moderately heavy labeling in a very small region. If the

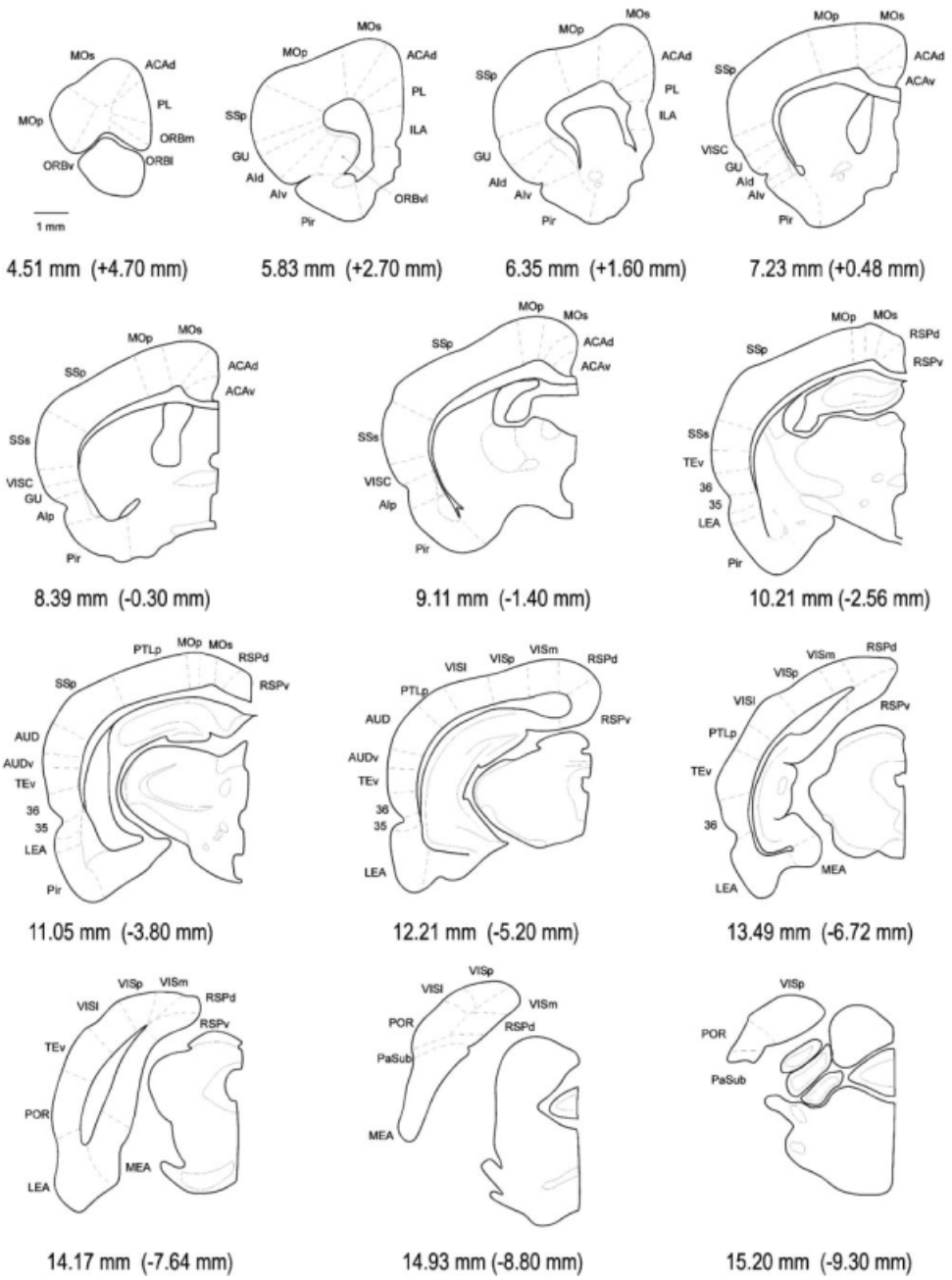

FIGURE 2. Cortical boundaries for all cortical regions quantified for a subset of coronal sections of a representative experimental brain. (Reproduced with permission from Burwell and Amaral, J Comp Neurol, 1998a, 398, 179–205, © Wiley-Liss) as the same regional boundaries were used for both studies. The first number represents the absolute rostrocaudal location of the plane of section (Swanson, 1992). The second number is coronal plane relative to bregma. Scale bar = 1 mm.

two regions are very different in volume the total fibers labeled will be very different. It could be argued that the size or overall strength of the projections differs. Thus, a second analysis took volume into account, to provide an assessment of the amount of label and the strength of the projection to each of the cortical regions analyzed. For this analysis, the density ratings in each cortical column were summed across the target region. To give an example, a target region with a volume of 1 unit and an average density of 3 would have a summed density of 3 following an anterograde injection in the region of origin. In comparison, a second target region with a volume of 3 units and an average density of 3 would have a summed density of 9. Even though the density of labeled fibers is the same in the two target regions, it could be argued that the projection to the second target regions is stronger.

These methods for quantifying fiber density and size of projections were specifically designed to provide a means for assessing the strength of connectivity as indicated by labeled

TABLE 2.

Mean Density of Labeled Fibers

Efferent regions	Origins				
	Area 36	Area 35	POR	LEA	MEA
Piriform	++	++	+	+++	++
Frontal					
MOs	++	++	+	++	+
MOp	+	++	+	++	+
PL	++++	+++	+	+++	+
ILA	++++	+++	+	+++	++
ORBm	+++	++	+	++	+
ORBl	+++	++	+	++	+
ORBvl	+++	++	++	++	+
Insular					
AId	+++	+++	+	+++	+
AIv	+++	+++++	+	+++++	++
AIp	++++	+++++	++	+++++	++
GU	+++	+++	+	++	+
VISC	+++	+++	–	++	+
Temporal					
AUD	+++	++	+++	++	+
AUDv	++++	+++	+++	++	+
TEv	+++++	+++	++++	++	++
Cingulate					
ACAd	++	++	++	++	+
ACAv	+	+	+	++	+
RSPd	+	+	+++	+	+
RSPv	+	+	++	+	+
Parietal					
PTLp	+++	++	++++	+	+
SSs	+++	++	+	++	+
SSp	++	++	+	++	+
Occipital					
VISl	+++	++	+++++	+	+
VISm	+	+	++++	+	+
VISp	+	+	+++++	+	+

Mean density of labeled fibers is the average density over the entire target region. The 5% of regions with the most dense labeling were designated very heavy (+++++); the next 5%, heavy (++++); the next 10%, moderately dense (+++), the next 30%, light; and the remaining 40% of the projections, very light (+).

fibers. We previously validated this method by examining the correlation between projection strengths assessed by mean density of labeled fibers following anterograde tracer injections with the mean estimated total cells labeled following retrograde tracer injections in six pathways (Kerr et al., 2007). The measures correlated were the summed densities of labeled fibers reported in this study and the estimates of total numbers of retrogradely labeled cells for the same pathways (Burwell and Amaral, 1998b). We were able to compare two sets of numbers for each of the projections (PER $\geq$ POR, POR $\geq$ PER, EC $\geq$ POR, POR $\geq$ EC, PER $\geq$ EC, and EC $\geq$ PER). Correlation analysis revealed a strong, linear correlation ($r = 0.77$) suggesting that this method of quantifying labeled terminal fibers following anterograde tract tracer injection, as we have employed it in these studies, is comparable to quantification by counting retrogradely-labeled cells. The high correlation also suggests that we were successful in discriminating terminal fibers from fibers of passage.

Finally, density of labeled fibers was also documented by photomicroscopy. Digital photomicrographs were taken on a Nikon E600 microscope interfaced with a SPOT RT digital camera (Diagnostic Instrument, Sterling Heights, MI). Images were adjusted for brightness and contrast. Composites were assembled in Adobe Photoshop. Text, laminar outlines, and borders were added using Canvas (Deneba Software, Miami, FL). No other adjustments were made to the images.

TABLE 3.

Summed Densities of Labeled Fibers

Efferent regions	Origins				
	Area 36	Area 35	POR	LEA	MEA
Piriform	94 ± 31	131 ± 63	25 ± 19	188 ± 60	59 ± 28
Frontal	223	207	58	189	26
MOs	79 ± 52	63 ± 38	27 ± 19	83 ± 68	8 ± 3
Mop	24 ± 19	61 ± 40	9 ± 4	34 ± 31	1 ± 1
PL	39 ± 13	35 ± 2	6 ± 3	23 ± 11	7 ± 3
ILA	19 ± 11	14 ± 4	1 ± 1	9 ± 4	5 ± 2
ORBm	16 ± 6	7 ± 2	3 ± 2	10 ± 4	0 ± 0
ORBl	23 ± 16	14 ± 8	8 ± 5	21 ± 14	1 ± 1
ORBvl	24 ± 11	14 ± 4	5 ± 4	9 ± 4	3 ± 2
Insular	124	144	18	121	33
AId	31 ± 11	29 ± 15	1 ± 1	26 ± 15	6 ± 3
AIv	12 ± 6	21 ± 7	2 ± 1	21 ± 6	8 ± 4
AIp	28 ± 9	37 ± 12	12 ± 6	40 ± 13	14 ± 6
GU	25 ± 8	26 ± 16	4 ± 1	16 ± 12	3 ± 2
VISC	29 ± 12	32 ± 22	1 ± 1	19 ± 16	2 ± 1
Temporal	187	98	163	53	49
AUD	42 ± 10	22 ± 9	45 ± 15	16 ± 10	12 ± 4
AUDv	30 ± 7	19 ± 8	18 ± 5	6 ± 3	5 ± 2
TE v	115 ± 29	58 ± 36	99 ± 12	31 ± 15	32 ± 11
Cingulate	47	34	163	64	47
ACAd	23 ± 11	21 ± 4	20 ± 12	25 ± 14	7 ± 5
ACAv	5 ± 3	9 ± 2	8 ± 4	9 ± 6	8 ± 5
RSPd	12 ± 5	3 ± 1	101 ± 40	13 ± 5	16 ± 4
RSPv	8 ± 3	2 ± 2	34 ± 6	16 ± 11	16 ± 8
Parietal	216	162	141	134	37
PTLp	36 ± 6	32 ± 21	76 ± 18	17 ± 11	12 ± 4
SS s	49 ± 36	21 ± 5	10 ± 4	25 ± 23	4 ± 3
SS p	131 ± 102	110 ± 40	55 ± 28	93 ± 88	20 ± 8
Occipital	52	40	281	19	23
VISl	36 ± 8	28 ± 21	106 ± 7	12 ± 7	11 ± 4
VISm	7 ± 5	5 ± 5	97 ± 45	4 ± 2	5 ± 3
VISp	10 ± 5	7 ± 6	78 ± 22	3 ± 2	6 ± 2

The summed density of labeled fibers is a function of the density of labeled fibers and the volume of the cortical termination region. These numbers represent the amount of fiber labeling resulting from injections in the region of interest. Data for individual regions are expressed as mean ± standard error. Means for composite areas are emboldened.

Confirmatory Data Analysis

To further validate our anterograde fiber labeling quantification method, we used classification data analysis techniques (Gordon, 1999). We previously applied this technique for connectional confirmation of our cytoarchitectural definitions of the PER and POR (Burwell, 2001). In this study, the question of interest was whether statistical classification based on patterns of cortical efferentation would correspond to regional location of the injection sites. If the two classifications converged, this would serve to validate the methods used to quantify labeled terminal fibers as well as inform interpretations of our results.

Cluster analysis was used to determine how anterograde tracer injection sites would be grouped based on the cortical patterns of labeled terminal fibers, but without information about the neuroanatomical location of the injection sites. The cluster analysis included all 20 injection sites. The variables entered into the analysis were the average density of labeled fibers in each of the 26 cortical areas for each injection site. The cluster algorithm we used was Ward's method. This is a hierarchical agglomerative (bottom up) method that is slightly biased toward producing clusters of the same size. Briefly, hierarchical agglomerative clustering begins with each case in a single cluster. In successive iterations, the closest pair of clusters is merged by satisfying a similarity criteria until all of the data is in one cluster. The similarity coefficient was euclidian distance. To identify the cluster solution (number of clusters), we plotted the number of clusters against *R*-squared and selected the number at which any further division would have relatively less effect on the amount of variance accounted for by the solution.

The cluster solution was then examined by multivariate analysis of variance (ANOVA) analysis of variance (MANOVA) to determine which variables (i.e., densities of labeling in a cortical region) significantly distinguished the clusters of injection sites. We then applied canonical discriminant analysis to determine the contribution of density of labeled fibers in the significant cortical regions upon the groupings of injection sites (Gordon, 1999). Discriminant analysis permits a visual representation of the cluster solution including how the cortical efferent variables relate to the clustering of injection sites.

RESULTS

Description of Injection Sites

The locations of individual injection sites within the PER, POR, and EC are shown in Figures 1B,C. Sites were distributed across all subdivisions and bands. Injection sites were defined as the region of cortex containing labeled cell bodies. Injection site size was quantified as the unfolded surface area using the same methods as was used in the unfolded maps. The injection sites for most cases were previously described in this manner (Burwell and Amaral, 1998b). Cases LEA 656B, MEA 652B, MEA 653B, and MEA 654B were unfolded using the same parameters. The laminar location and the unfolded surface area of the injection sites in each parahippocampal region are presented in Table 1. One issue is the concern that the strength of labeling depends on the size of the injection site. A case-by-case review of injection size and total labeling indicated that the amount of labeling was not related to the size of the injection site.

Of the PER cases, one injection site (case 54P) was restricted to deeper layers (Table 1 and Fig. 1C). All others penetrated deep and superficial layers. One of the POR injection sites was also restricted to deep layers (83B). Two LEA sites were largely located in superficial layers (61B and 66P). There were labeled cells in layers V and VI for each of these two cases, but by our estimates the proportion was less than one-third of the total labeled cells. The cells labeled in deep layers, however, were more dispersed and were located on the outer edges of the injection site. Thus, they may have given rise to more efficient labeling. This is important to note because the cortical efferents arise in deep layers (Insausti et al., 1997). For the remaining four injection sites labeled cells were distributed across deep and superficial layers. Two sites in the LEA encroached slightly on PER area 35 (cases 127B and 61B). All other injection sites were located entirely in the intended region. Of the MEA cases, three injections were restricted to deep layers and two penetrated deep and superficial layers.

Regarding EC subregions, injection sites were distributed across the subdivisions as defined by Insausti et al. (1997), the dentate gyrus projecting bands, and the LEA and the MEA.

Pathways

The cortical efferents arising from the PER, POR, and EC tended to follow similar axonal trajectories. Most fibers emerging from injection sites traveled away from the pial surface to enter the external capsule. After traveling through the external capsule, labeled fibers exited to innervate cortical target regions. A smaller complement of labeled fibers coursed superficially and traveled through layer I to innervate regions both anterior and posterior to the injection site. Although contralateral projections were not quantified in this article, we did examine the pathways of contralateral connections. Fibers of passage were observed to cross to the hemisphere opposite the injection site via the corpus callosum and the temporal limb of the anterior commissure. Fibers traveling to the contralateral hemisphere largely targeted the region homotopic to the location of the injection site.

Overview

Preliminary analyses indicated differences in density of labeled fibers resulting from injection sites in the PER areas 35 and 36. For that reason, and to be consistent with prior studies, area 35 and 36 experiments were evaluated separately. A similar situation emerged for entorhinal subdivisions, LEA and MEA. Thus, density of labeled fibers was quantified for five regions: area 36, area 35, POR, LEA, and MEA. A summary

of the results is presented in Tables 2 and 3. In general, tracer injections located in the PER and POR resulted in more labeled fibers than tracer injections located in the LEA and MEA. It should be noted, however, that only one injection site in the LEA lateral band included the deep layers. As might be expected, the site that included all layers produced more labeling in cortical regions. Nevertheless, injections located in the LEA lateral band produced densities of labeled fibers comparable to that of injection sites located in area 36 and the POR. Tracer injections located in the MEA resulted in the least amount of labeled fibers. Although not shown separately in the tables, we also discuss differences in labeling resulting from entorhinal injection sites based on the DG-projection band of origin (Fig. 1B).

As discussed earlier, the two measures used to quantify labeled fibers provide different information. The mean density of labeled fibers (Table 2) is independent of the size of the target region. In contrast, the summed density of labeled fibers shown in Table 3 reflects the amount of label in the entire structure arising from a single injection site, and thus may provide a better measure of the strength of a whole projection from that location.

Perirhinal Cortex

PER injection sites resulted in substantial labeling of fibers in a number of neocortical association regions. With some notable exceptions, injection sites located in area 36 resulted in slightly more labeled fibers than injection sites located in area 35 (Tables 2 and 3). Insular regions were more heavily targeted by area 35. Frontal, temporal, and parietal regions, including secondary somatosensory cortex, tended to be more heavily targeted by area 36. For both regions, rostral injection sites resulted in heavier densities of labeled fibers, overall, than caudal injection sites. Labeling in sensory regions exhibited a strong topography. The heaviest labeling in somatosensory cortex resulted from rostral PER sites, the heaviest labeling in auditory regions resulted from mid-rostrocaudal PER sites, and the heaviest labeling in visual regions resulted from caudal PER (Fig. 3). In general, the laminar patterns of labeled fibers were similar across target regions. Layers I, II, and VI were more likely to be labeled than III and V.

The data suggest that the heavier projections terminate in PIR, frontal, and temporal regions; weaker projections terminate in cingulate and occipital regions. Although the intensity of labeling was greater from area 36 sites, the location of cortical labeling arising from PER area 36 and 35 injection sites was similar. As is evident in the following sections, however, detailed analyses revealed subtle differences in both the topography and the laminar patterns of terminal labeling.

Piriform region

Anterograde injection sites in rostral PER resulted in light density labeling in PIR, on average (Table 2). Because the PIR is relatively large, however, the total fiber labeling revealed a substantial amount of labeled fibers in the region taken as a whole (Table 3). Examination of individual cases revealed that lightest density of labeled fibers arising from area 36 resulted from the most caudal injection (Fig. 3). The same pattern was true for the most caudal injection site in area 35. There were differences in the topography. Injection sites in area 35 tended to produce labeling in all rostrocaudal levels of PIR. In contrast, sites in area 36 showed a topography such that more rostral sites produced more labeling in rostral PIR and more caudal sites produced more labeling in caudal pirform cortex. Regardless of the area of origin, labeled fibers were observed in all layers of the PIR. Labeling was heaviest in I and III, but some fibers were observed to penetrate layer II.

Frontal regions

Injections in areas 35 and 36, resulted in substantial labeling in frontal regions, with area 36 sites resulting in more labeling overall (Tables 2 and 3). In general, the more rostral injection sites in areas 35 and 36 produced denser labeling than more caudal sites (Fig. 3). The most caudal site in area 36, however, produced scant labeling in frontal regions. Area 36 sites resulted in more labeling than area 35 sites, with the exception of MOp, which was more heavily labeled by area 35 sites. The total amount of labeled fibers was greatest in primary and supplementary motor regions (MOp and MOs, Table 3). This is because of the size of those regions. The mean density of labeling in these regions, however, was relatively light (Table 2). The heaviest labeling was in layers I and VI, but there was light labeling observed in layers II–V.

Mean density of labeled fibers in the prelimbic and infralimbic regions was moderately heavy following area 36 injections and moderate following area 35 injections. There was no clear topography of area 35 labeling; both the rostral and the caudal site produced similar patterns. Area 35 injection sites preferentially labeled layers II–V of the infralimbic cortex, but labeling was also observed in deep layer I and layer VI (Fig. 4B). More caudally, labeled fibers in the prelimbic and infralimbic cortices resulting from tracer injections in area 35 exhibited more of a split laminar pattern such that labeling was greater in layers I–II and in VI. There was some evidence for a topography of area 36 labeling such that rostral sites produced heavier labeling and the caudal site produced very little labeling in either region (Fig. 3). In addition, the more rostral area 36 site targeted rostral PL more strongly and the mid-rostrocaudal sites targeted ILA more strongly. Infralimbic labeling following rostral area 36 injections was observed in all layers but was heavier in layers II–III (Fig. 4C). More caudal sites resulted in heavier labeling in VI as well as II–III.

Perirhinal labeling in orbital frontal regions varied from light to moderately heavy. Injections in area 36 resulted in heavier labeling in orbital regions as compared to area 35 (Tables 2 and 3). Moreover, the area 36 labeling showed a topography such that the rostral site produced more labeling than the caudal sites. That topography was not observed for area 35 sites; both the rostral and caudal sites produced similar

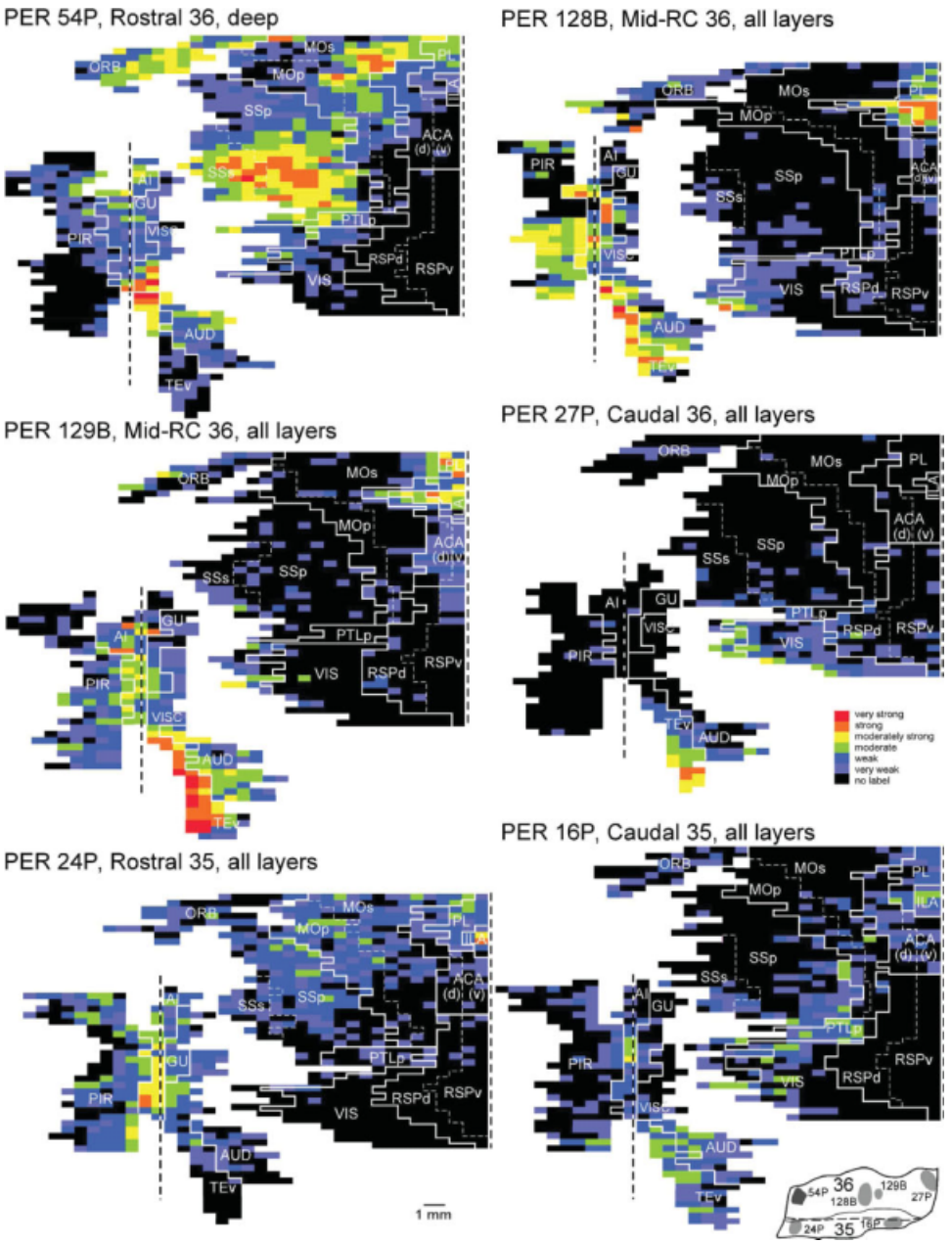

FIGURE 3. Unfolded maps of the density of labeled fibers resulting from injection sites in the PER. Each case is identified by case number, location, and laminar position of the injection site (see icon in lower right corner). Two unfolded maps were constructed. The piriform, insular, and temporal regions were unfolded relative to the rhinal fissure (lower left of each panel). The frontal, cingulate, parietal, and visual regions were unfolded relative to the midpoint (upper right of each panel). Some regions were combined to simplify the maps. For each case, voxels were scored on a density scale from heaviest (6, red) to lightest (1, purple). Voxels in which there was no labeling are black in the figure. In general, labeling was heavier following area 36 than area 35 injections. For both regions there was a rostrocaudal topography in the patterns of terminal labeling. See list for abbreviations. [Color figure can be viewed in the online issue, which is available at www.interscience.wiley.com.]

patterns of labeling. For all sites, labeled fibers were observed in all layers, but were heavier superficial layers and in layer VI (Fig. 5).

Insular regions

Labeling in insular regions following PER injections was substantial. The density of labeled fibers in all insular regions was heavier following tracer injections to rostral PER (Fig. 3). In contrast to most other projections, density of labeled fibers arising from area 36 was not uniformly heavier than density of labeled fibers arising from area 35 (Tables 2 and 3). Density of labeled fibers was heavy in AIv and AIp and moderate in the other regions following area 35 injections. Area 36 injections produced moderate labeling in all regions except AIp in which labeling was moderately heavy.

Following area 35 injections, fibers were observed in layers II–V of insular cortex. Following area 36 injections, however, fiber density in AId was greatest in layers I–III rostrally, and shifted to layers V–VI in caudal insular areas. In AIp, density of labeled fibers was heaviest in layer VI and lightest in superficial layers. Density of labeling in layer V was somewhere in between. The density and patterns of labeled fibers in the

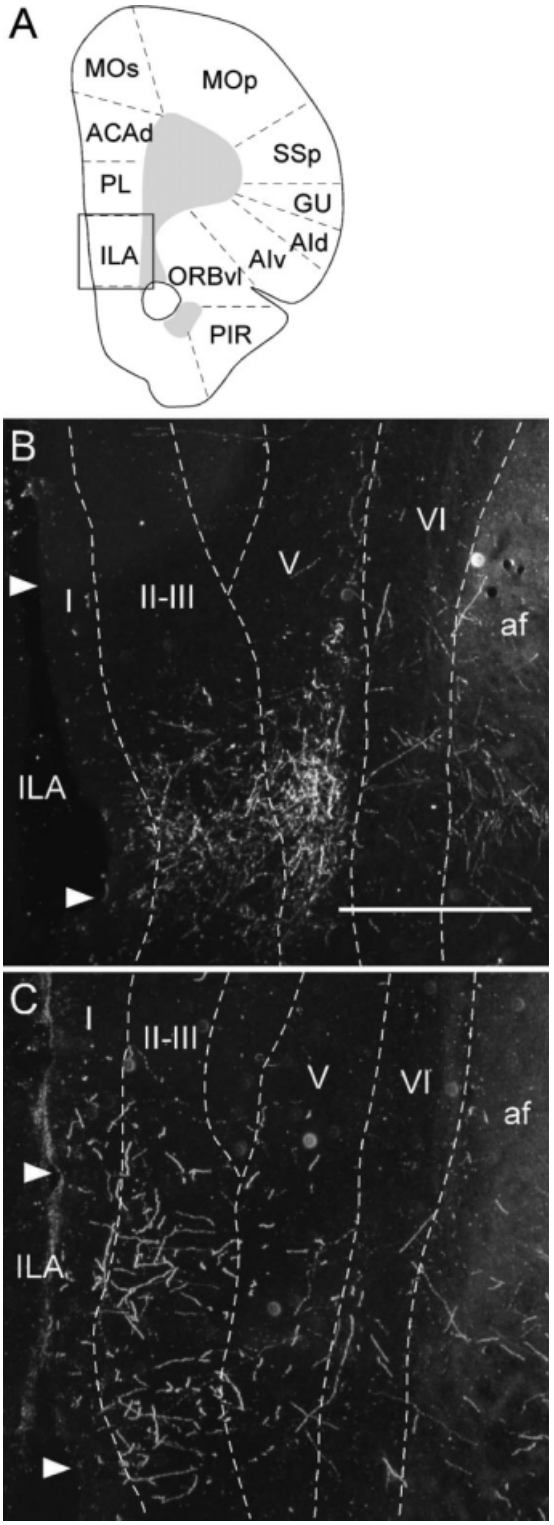

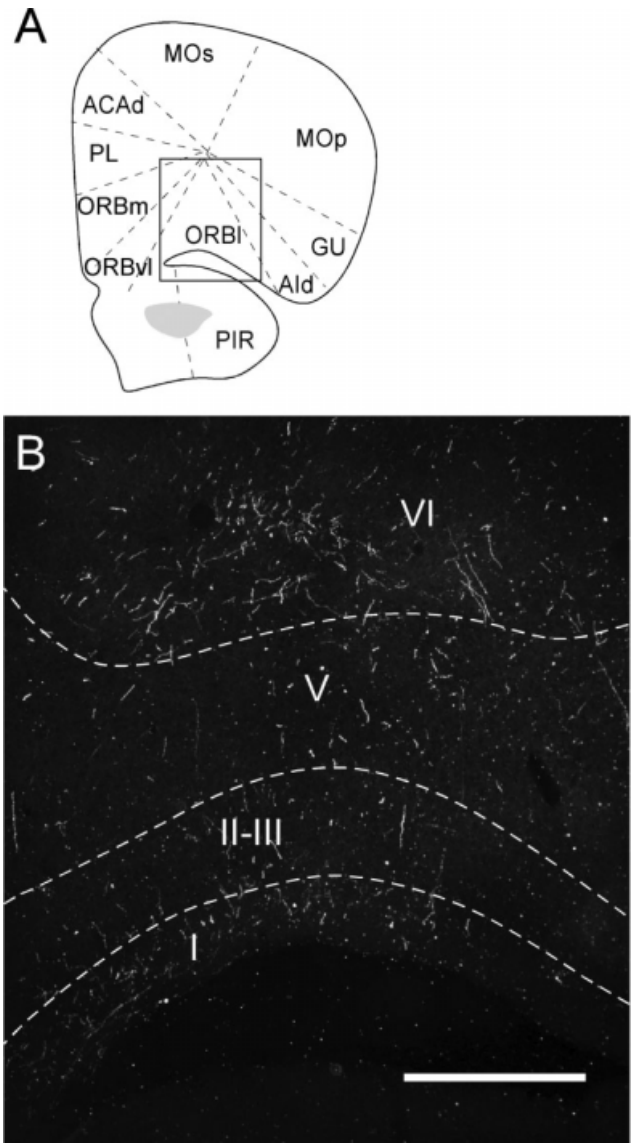

FIGURE 5. Labeling in lateral orbital frontal cortex following an injection in mid-rostrocaudal PER area 36. (A) Schematic showing the coronal level of the photomicrograph. (B) Darkfield photomicrograph showing the pattern of labeled fibers (case 54P). Labeled fibers were observed in all layers. Scale bar: 500 μm.

FIGURE 4. Labeling in the infralimbic cortex (ILA) following PER injections. (A) Schematic of a coronal section showing the location of the accompanying darkfield photomicrographs (inset). (B) Darkfield photomicrograph showing labeled fibers resulting from a tracer injection in rostral PER area 35 (case 24P). This particular section shows an area of relatively heavy labeling for this particular case. Fibers were observed to terminate in all layers of the ventral IL, but were heaviest in layer III and especially V. Little to no fiber labeling was observed in PL. (C) Labeled fibers resulting from a tracer injection in mid-rostrocaudal area 36 (case 128B). Labeling was observed in all layers, but was heaviest in layers II–III and of the IL. Scant labeling was observed in PL. af, anterior forceps of the corpus callosum. Scale bar: 500 μm.

granular insular regions was similar for area 36 and area 35 injections; labeled fibers in visceral and gustatory regions were observed in deep and superficial layers of cortex. In some cases, layer I labeling was heaviest and in others layer VI labeling was heaviest.

Temporal regions

Density of labeled fibers in temporal regions following PER injections was substantial, although area 36 sites resulted in more labeling than area 35 sites (Fig. 3). The density of labeling ranged from moderate to heavy for area 36 injection sites and from light to moderate for area 35 injection sites. In terms of quantity of input to temporal regions, the majority of fibers terminated in TEv (Table 3).

The pattern of labeling in TEv showed an interesting topography. Rostral sites preferentially labeled rostral TEv and caudal sites preferentially labeled caudal sites. The sites located in mid-rostrocaudal area 36, however, produced strong labeling in the full rostrocaudal extent of TEv (Fig. 3). This topography was not observed for area 35 sites. Though the density was weaker overall, rostral TEv was preferentially labeled regardless of rostrocaudal location of the injection site. Labeled fibers were observed largely in all layers of TEv, but labeling was heavier in layer I and in layers VI.

Following injection sites in mid-rostrocaudal area 36, moderately heavy density of labeled fibers was observed in ventral auditory cortex (Table 2), which is auditory association cortex. In terms of amounts of labeling, the indexes were higher for dorsal auditory regions than in ventral regions (Table 3). This is because primary auditory cortex is substantially larger than ventral auditory cortex yielding larger numbers for total amount of labeling. Layers I–III and VI were preferentially labeled, but labeled fibers were observed in layers IV and superficial V (Fig. 6).

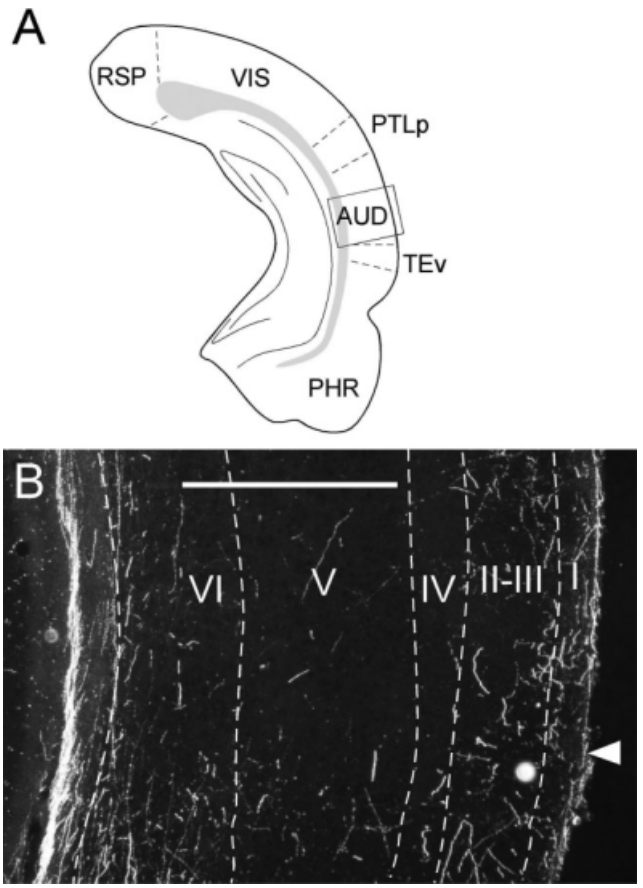

FIGURE 6. Labeling in auditory cortex following an injection in mid-rostrocaudal PER area 36. (A) Schematic showing the level of the photomicrograph. (B) Darkfield photomicrograph showing the distribution of labeled fibers in auditory cortex (case 128B). Fibers terminate preferentially in deep and superficial layers. AUDv is below the arrow. Scale bar: 500 µm.

Cingulate regions

Observed mean density of labeled fibers suggests that PER provides relatively weak input to cingulate and retrosplenial regions (Tables 2 and 3). The unfolded maps, however, reveal that there is a modest projection from rostral area 36 to rostral ACAd. Interestingly, there were very few labeled fibers in the retrosplenial cortex. The most labeling was observed in caudal RSPd as a result of a caudal area 36 injection. Area 35 injections produced little or no retrosplenial labeling. For both area 35 and area 36 injection sites, the majority of labeled fibers were in superficial layers.

Parietal regions

Here we included the primary and secondary somatosensory regions with the posterior parietal cortex, which is a polymodal associational region. Thus, we will cover the two areas separately. Parietal regions exhibited light to moderate density of labeled fibers following tract tracer injections located in areas 35 and 36 (Table 2). Density of labeled fibers in primary and secondary somatosensory cortex was light overall, but was heavier following rostral PER injections, especially following injections in area 36 (Fig. 3). Terminal labeling was observed in layers I–III and was greater in caudal portions of somatosensory regions. The amount of labeled fibers revealed that the greatest amount of parietal labeling following PER injections targeted SSp, which is the largest parietal region (Table 3). For the somatosensory regions, the PER receives more input from SSs. Given that the projections are likely to be reciprocal, it might be expected that the secondary region, SSs, would be more heavily labeled than the primary region, SSp, but with the exception of one case, this was not the pattern. Case PER 24 exhibited stronger labeling in SSp than in SSs (Fig. 3).

The density of labeled fibers in PTLp was slightly greater following area 36 injections as compared to area 35 injections (Tables 2 and 3). The rostral area 36 injection site produced more labeling in the dorsal limb, whereas the more caudal sites produced more labeling the caudal limb. Following area 35 injection sites, labeled fibers were more homogeneously distributed in the dorsal and caudal limbs. The more caudal injection site in area 35 produced more label overall. Fibers were observed to

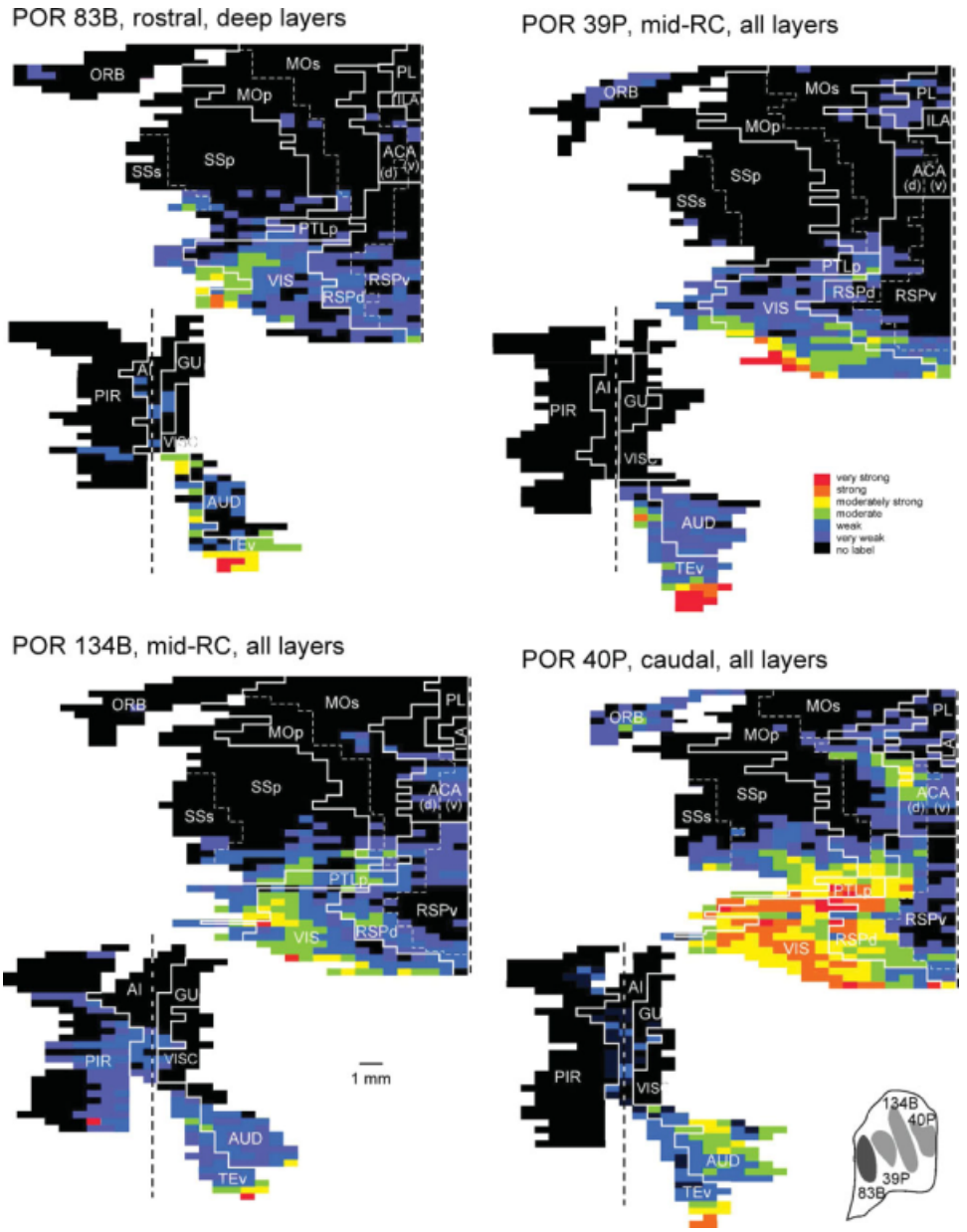

FIGURE 7. Unfolded maps of the density of labeled fibers resulting from injection sites in the POR. Each case is identified by case number, location, and laminar position of the injection site (see icon in lower right corner). Voxels in which there was no labeling are black in the figure. Injections in all rostrocaudal levels of POR produced labeled fibers in caudal TEv and visual cortex. The more caudal the injection site, the heavier the labeling in visual regions. See list for abbreviations. [Color figure can be viewed in the online issue, which is available at www.interscience.wiley.com.]

terminate preferentially in superficial layers regardless of whether the injection site was located in area 35 or area 36.

Occipital regions

Density of labeled fibers in visual regions ranged from very light to moderately dense. Density of labeled fibers was heaviest by far in lateral visual association cortex, especially following injections in area 36 (Tables 2 and 3). Stronger innervation of all occipital areas originated in caudal PER for both area 35 and area 36 injections (Fig. 3). Labeled fibers were restricted to superficial cortical layers. Although area 36 injections produced more labeled fibers in occipital regions, the laminar pattern of labeled fibers was similar for area 35 and 36 injections.

Postrhinal Cortex

As a general principle, POR injections tended to produce more labeling in caudal than rostral cortical regions (Fig. 7). The patterns of labeled fibers suggest that the heavier projections terminate in dorsal retrosplenial, posterior parietal, visual, and ventral temporal regions (Tables 2 and 3). The labeling in

frontal and insular regions was much weaker, though there was labeling in orbital prefrontal and anterior cingulate regions. Interestingly, there was a modest but notable amount of labeling in auditory cortex. Thus, in terms of input to sensory regions, the main targets of POR are visual, visuospatial, and auditory cortices. Only weak labeling was observed in somatosensory, olfactory, and gustatory regions.

Piriform regions

POR injections resulted in only very light innervation of PIR, overall (Tables 2 and 3). Only one injection site resulted in PIR labeling. That site was located in caudal POR, but covered dorsal and ventral levels and included all layers. Labeled fibers were located in the most caudal portions of the PIR in layers I and III (Fig. 7).

Frontal regions

Density of labeled fibers in frontal regions was modest. Overall, POR innervation of frontal regions was very light (Tables 2 and 3). The region exhibiting the densest labeling was ORBvl (Table 2). There was an evident topography. The most caudal injection site produced more labeling in orbital regions than other sites, and ORBvl was preferentially labeled (Fig. 7). The region exhibiting the most labeling, as indicated by summed density of labeled fibers, was MOs (Table 3). Again, the most caudal injection site was largely responsible for the MOs labeling, There was little or no labeling in MOp arising from any injection site. Labeled fibers in all frontal regions targeted superficial layers.

Insular regions

Density of labeled fibers in insular regions resulting from POR injections was minimal. The density of labeling ranged from absent to light (Table 2). The summed density of labeled fibers was also very low, with the most labeling observed in AIp followed by GU (Table 3). Labeling in the insular regions originated largely from caudal POR injection sites, and primarily targeted AIp and posterior GU. Labeled fibers were observed primarily in deep layers (Fig. 7).

Temporal regions

The patterns and density of labeled fibers in temporal regions following POR tracer injection suggest that the projection to temporal regions is substantial overall, especially to TEv. Densities and amounts of labeling were exceeded only by labeling in occipital regions (Tables 2 and 3). The density of labeled fibers in TEv following POR tracer injections was moderately heavy, overall (Table 2). The strongest labeling was in caudal ventral temporal cortex (Fig. 7). Closer to the injection site, labeled fibers preferentially targeted layers I–III and VI. More rostrally, and farther away from the injection site, labeling was still observed in all layers, but was heavier in layer VI (Fig. 8C).

The density and amount of labeled fibers in auditory regions suggest that the POR projection to auditory regions is of moderate strength (Tables 2 and 3). On the basis of patterns of labeled fibers, there is a rostrocaudal topography of the POR projection to auditory cortex. All rostrocaudal levels of POR appear to project to auditory cortex, but as the more caudal the location of the injection site, the heavier the labeling in auditory cortex (Fig. 7). Labeled fibers were observed in superficial layers of cortex.

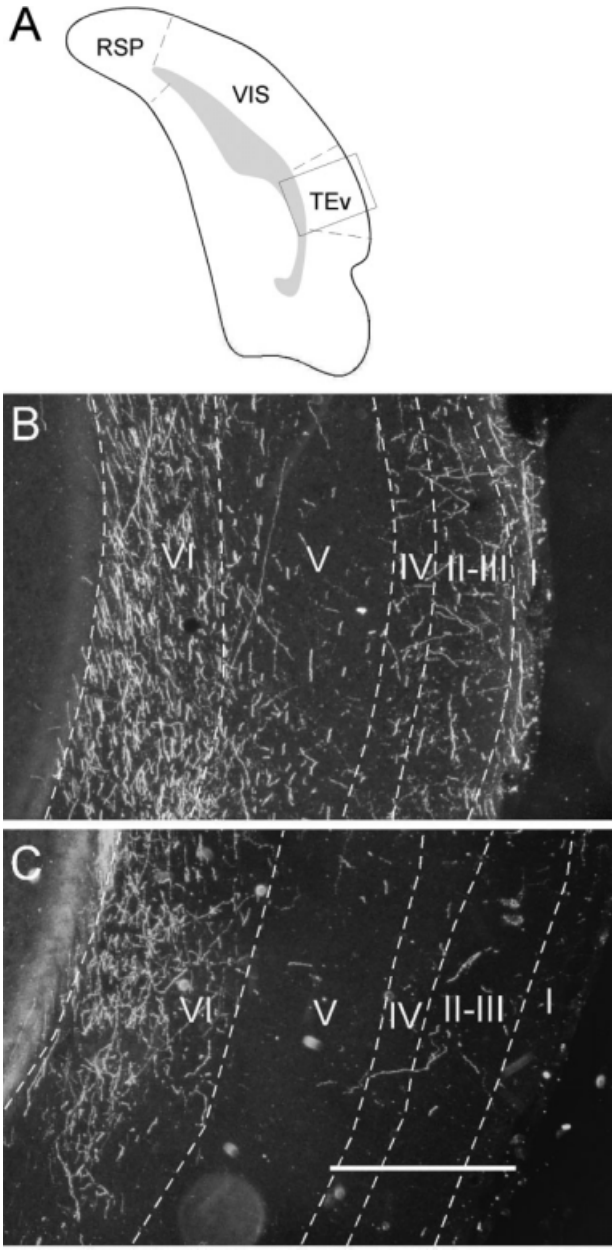

FIGURE 8. Labeling in TEv following PER and POR injections. (A) Schematic showing the location of the darkfield photomicrographs. (B) Labeled fibers following a tracer injection to mid-rostrocaudal PER area 36 (case 128B) were heaviest in layerVI, moderate density of labeled fibers is observed in superficial layers, and in V to a lesser extent. (C) Labeled fibers resulting from anterograde tracer injection to caudal POR (case 39P). Fibers terminate preferentially in deep layer VI. Scale bar: 500 µm.

Cingulate regions

POR appears to provide a substantial projection to cingulate regions that preferentially targets retrosplenial areas (Fig. 7). Following POR injections, the mean density of labeling was moderate in RSPd and light in RSPv. The amount of labeled fibers suggests that the largest projection targets RSPd (Table 3, note that RSPv is closer to the midline). There was a topography such that the rostral sites gave rise to lighter labeling and more caudal injection sites gave rise to more extensive and denser patterns of labeling. The densest labeling was observed in RSPd following the most caudal injection site. Labeled fibers terminated primarily in layers I–II, but also in deep layers (Fig. 9B). In anterior cingulate cortex, the density of labeling was light in ACAd and very light in ACAv following injections in the POR (Table 2). The same pattern was evident in the amount of labeled fibers in the two regions (Table 3). There was a topography such that caudal POR injection sites produced more labeling than rostral sites (Fig. 7). In addition, the heaviest labeling was observed in the caudal portion of the region. Labeled fibers were observed in all layers, but was heavier in layers I, II, and deep VI (Fig. 9B).

Parietal regions

Somatosensory regions appeared to receive very little direct input from POR. Densities of labeled fibers in both primary and supplementary somatosensory cortex were very light (Table 2). The amount of labeled fibers was relatively small given the size of the regions, especially for SSs (Table 3). The amount of labeling in the somatosensory regions following POR injections was less than any other projection region with the exception of the MEA. The unfolded maps suggest that the projection shows a rostrocaudal topography. The more caudal the injection site, the heavier the labeling. Density of labeled fibers was heaviest in caudal SSp. Labeled fibers were observed, primarily in layers I–III and VI. Layer V was lightly labeled in some sections.

The mean density of labeling in PTLp was as heavy as any other region with the exception of visual cortex. Moderately heavy densities of labeled fibers were observed in posterior parietal regions (Table 2). The amount of labeled fibers in PTLp produced by POR injections was more than twice that produced by any other region (Table 3). Caudal POR injection sites gave rise to heavier labeling than did rostral POR sites (Fig. 7). Labeled fibers in rostral posterior parietal regions terminated in superficial layers of cortex. In the caudal limb of posterior parietal cortex, which exhibited the heaviest labeling, fibers were observed in all cortical layers (Fig. 9D). Labeled fibers were heaviest in layer I, deep V, and VI. Layers II–IV and superficial V were more lightly labeled.

Occipital regions

Overall, the greatest amount and the heaviest densities of labeling following POR injections were in occipital regions (Tables 2 and 3). POR injection sites resulted in moderately heavy to heavy densities of labeled fibers in primary and secondary visual regions. On the basis of the mean densities and summed densities of labeled fibers, the projection to visual association cortex appears stronger. The patterns of labeled fibers showed a topography such that the more caudal the injection site the heavier the density of labeled fibers, especially in VISl (Fig. 7). In general, labeled fibers were heaviest in

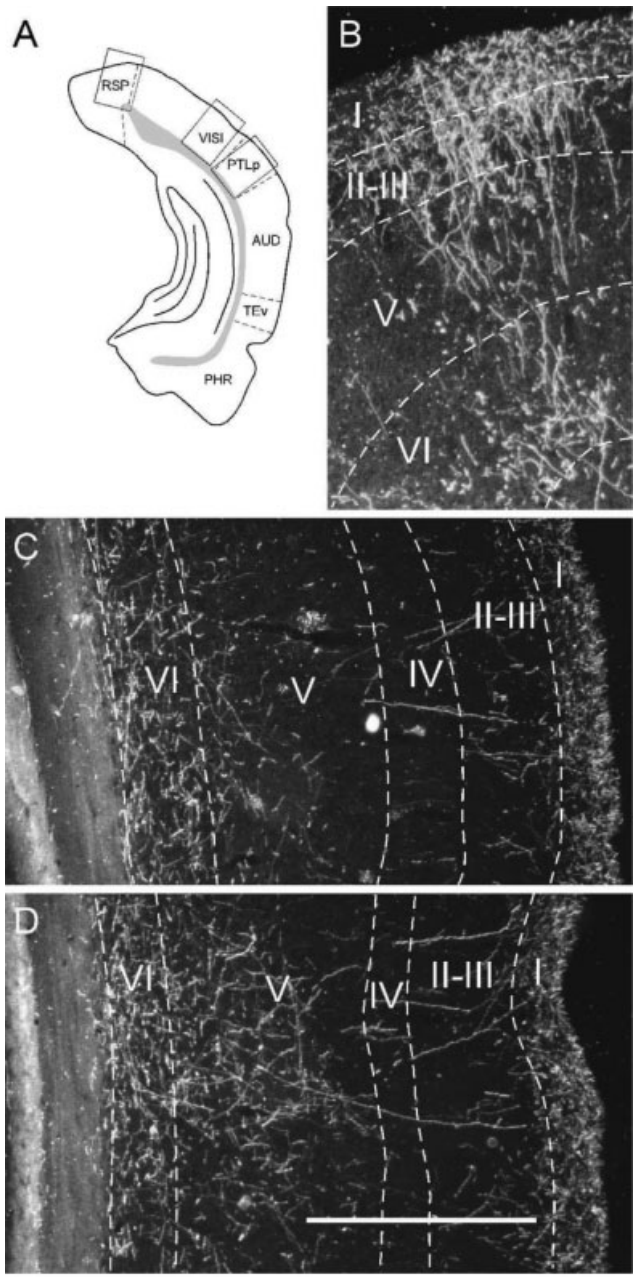

FIGURE 9. Labeling in posterior cortical regions following a POR injection (case 39P). (A) Schematic showing the level and location of the darkfield photomicrographs in panels (B)–(D). (B) Fibers were observed in all layers of retrosplenial cortex, but were heaviest in layers I-II. (C) Labeling in lateral visual cortex was observed in all layers, but was heavy in layers I and VI. (D) Labeled fibers in the posterior parietal cortex were observed in all layers, but were most dense in layers I, deep V, and VI. Scale bar: 500 μm.

layers II–III, deep V, and VI. In more caudal regions, however, dense fiber labeling was observed in all cortical layers; similar to the pattern of labeling in PTLp, layers I, deep V, and VI exhibited heavier labeling, and layers II–IV and superficial V were more lightly labeled (Fig. 9C).

Entorhinal Cortex

Analysis of the patterns of labeled fibers produced by EC injections revealed several principles. Overall, tract tracer injections located in the EC tended to produce less labeled fibers in cortical regions as compared to the PER and POR (Tables 2 and 3), even when taking the injection site layers into account. Within the EC, injection sites located in the LEA produced substantially more labeling than injection sites located in the MEA. Moreover, injection sites in LEA and MEA gave rise to qualitatively different patterns of labeling in cortical regions. LEA injections located in the lateral band tended to give rise to more labeled fibers in cortical regions. Band of origin has less impact on the patterns and density of labeling for the MEA sites. Instead, the ventrally located MEA injection sites produced more cortical labeling regardless of the band of origin.

The heaviest labeling resulted from an injection located in the rostral part of the lateral band of the LEA (Fig. 10). For the other two lateral band injection sites, the majority of the filled cells at the injection site were located in superficial layers, which may account for the more limited labeling. It should be noted, however, that both of those injection sites included labeled cells in layers V and VI, so some amount of labeling in cortical regions would be expected. For the MEA, the density of labeled fibers in all 26 regions was either weak or very weak (Table 2). All MEA injection sites involved deep layers. Thus, laminar location of the injection sites cannot explain the light labeling. In general, the amount of labeling was about three times greater for injection sites in the LEA as compared to the injections sites in the MEA (Table 3). For both subdivisions, the largest amount of labeling was observed in PIR. PIR labeling aside, the relative ranking of the other targeted regions based on summed densities of labeled fibers were strikingly different for the LEA and MEA injections. For example, MEA injections (Fig. 11) produced relatively more labeling in ventral temporal, retrosplenial, and posterior parietal cortices, whereas the LEA (Fig. 10) injections produced relatively more labeling in frontal and insular regions.

Piriform regions

On the basis of the summed densities, the entorhinal injection sites gave rise to labeling of more terminal fibers in to PIR than any other region. This was true for both LEA and MEA, though the amount of labeled fibers observed in LEA was substantially greater than that of the MEA. Tracer injections in the LEA resulted in moderately dense fiber labeling in PIR, overall, (Table 2), but PIR labeling ranged from weak to heavy depending on the location of the injection site and the terminal labeling. Injections in the lateral band of the LEA resulted in the heaviest labeling (Fig. 10, case 127). Tracer injections to the intermediate and medial bands of the LEA gave rise to very weak labeling that terminated preferentially in dorsal PIR (Fig. 10). Fibers preferentially targeted layers I and III of PIR, but fibers were occasionally visible in layer II (Fig. 12).

Overall, the density of PIR labeling following MEA injections was light as compared to the moderately dense labeling following LEA injections (Table 2). Ventrally located sites (cases 652, 653, and 654) produced more labeling regardless of the band of origin (Fig. 11). The most lateral and the most medial sites in the lateral band produced almost no labeling (Fig. 12C). Following injections in LEA or MEA, labeling was heaviest in dorsal and caudal PIR. Similar to the LEA sites, MEA sites labeled layers I and III of PIR with scattered fibers in layer II.

Frontal regions

The density of labeled fibers in frontal regions ranged from very light to moderate depending on the region and on the location of the injection site (Table 2). On the basis of the summed densities, LEA injection sites produced more labeling than MEA sites in all frontal regions (Table 3). Following LEA injections, labeled fibers in the PL and the ILA were moderately dense. The injection sites in the lateral band gave rise to heavier labeling. There was a topography such that the rostral site in the lateral band gave rise to heavier labeling in the PL and the caudal site gave rise to heavier labeling in the ILA. For PL and ILA, labeling tended to be heavier in layers I–III, though in some cases lighter labeling was observed in deeper layers. Labeling following MEA injections was light, but similar to the patterns of PIR labeling, the more ventrally located MEA sites produced more PL/ILA labeling.

Labeling in orbital frontal regions was light following LEA injections and very light following MEA injections (Table 2). The most rostral LEA lateral band site gave rise to heavier labeling in ORBl (Fig. 10). Otherwise there was no topography to the projections.

As might be expected, the larger quantity of fibers was observed in the larger motor regions, MOs and MOp (Table 3). Only the most rostral LEA site in the lateral band produced substantial labeling in these regions, and labeling in the MOs was greater than labeling in the MOp (Table 3). For MEA sites, only the most medial site, which was also in the lateral band, produced much labeling in motor regions (Fig. 11).

The laminar patters of labeling were largely similar for LEA and MEA sites. Labeling in motor regions targeted layers I and VI. Labeling in PL/ILA and the orbital regions preferentially targeted layers I–III and was relatively lighter in deeper layers.

Insular regions

The LEA injection sites produced heavy labeling in agranular insular regions and moderately dense labeling in granular regions (Table 2). The overall amount of labeling was greatest in AIp and was similar in other regions (Table 3). Moreover, LEA sites in the lateral band gave rise to more labeling in insular regions, especially the rostral part (Fig. 10). Labeling in agranular insular regions was observed in all layers, but there

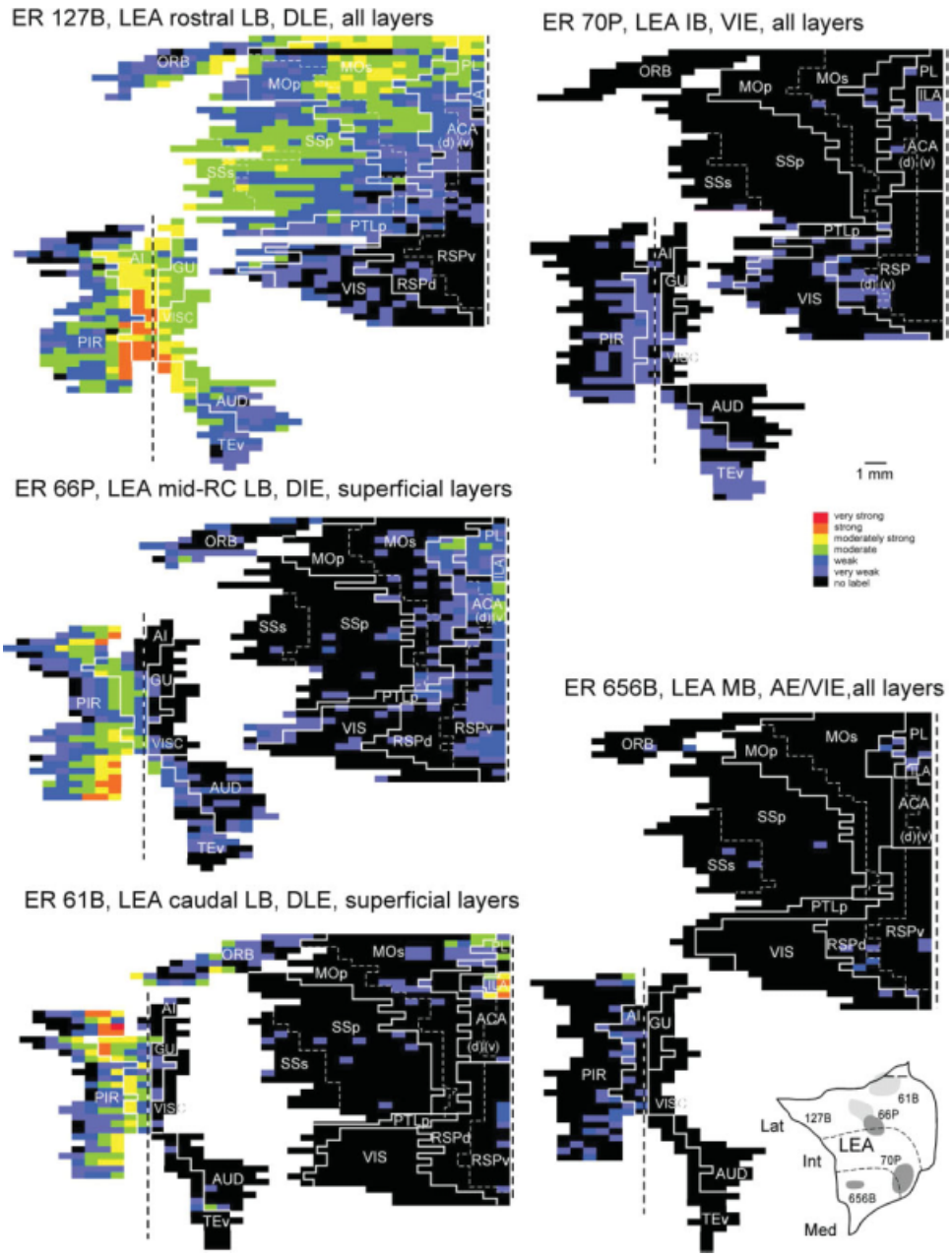

FIGURE 10. Unfolded maps of the density of labeled fibers resulting from injection sites in the lateral entorhinal area (LEA). Maps are labeled with the case name, location, band, and layers involved in the injection site (see icon in lower right corner). Voxels in which there was no labeling are black in the figure. The heaviest labeling resulted from injections in the lateral band (LB), especially the rostral LB. However, it should be noted that the rostral site involved all layers and the med-RC and caudal sites involved only superficial layers. Because the cortical efferents arise in deep layers, it might be expected that labeling would be weaker. Rostral injection sites targeted frontal, insular, piriform, and anterior cingulate areas. Labeling following injections in the intermediate and medial bands (IB and MB) was substantially weaker. [Color figure can be viewed in the online issue, which is available at www.interscience.wiley.com.]

was a laminar distribution. Fibers in the superficial layers, layers I-III, formed a dense plexis. Labeling in deeper layers, V and VI, was progressively lighter.

In contrast to LEA sites, tracer injections located in the MEA resulted in light or very light labeling in insular regions (Tables 2 and 3). Although density of labeled fibers was weak overall, the heaviest labeling was produced by the injection site that was located in the medial band (Fig. 11). Overall, the greatest amount of labeled fibers was observed in the AIp (Table 2). In general, labeled fibers were located in deep layers.

Temporal regions

Labeling in ventral temporal and auditory areas was light following LEA injections and light or very light following MEA injections

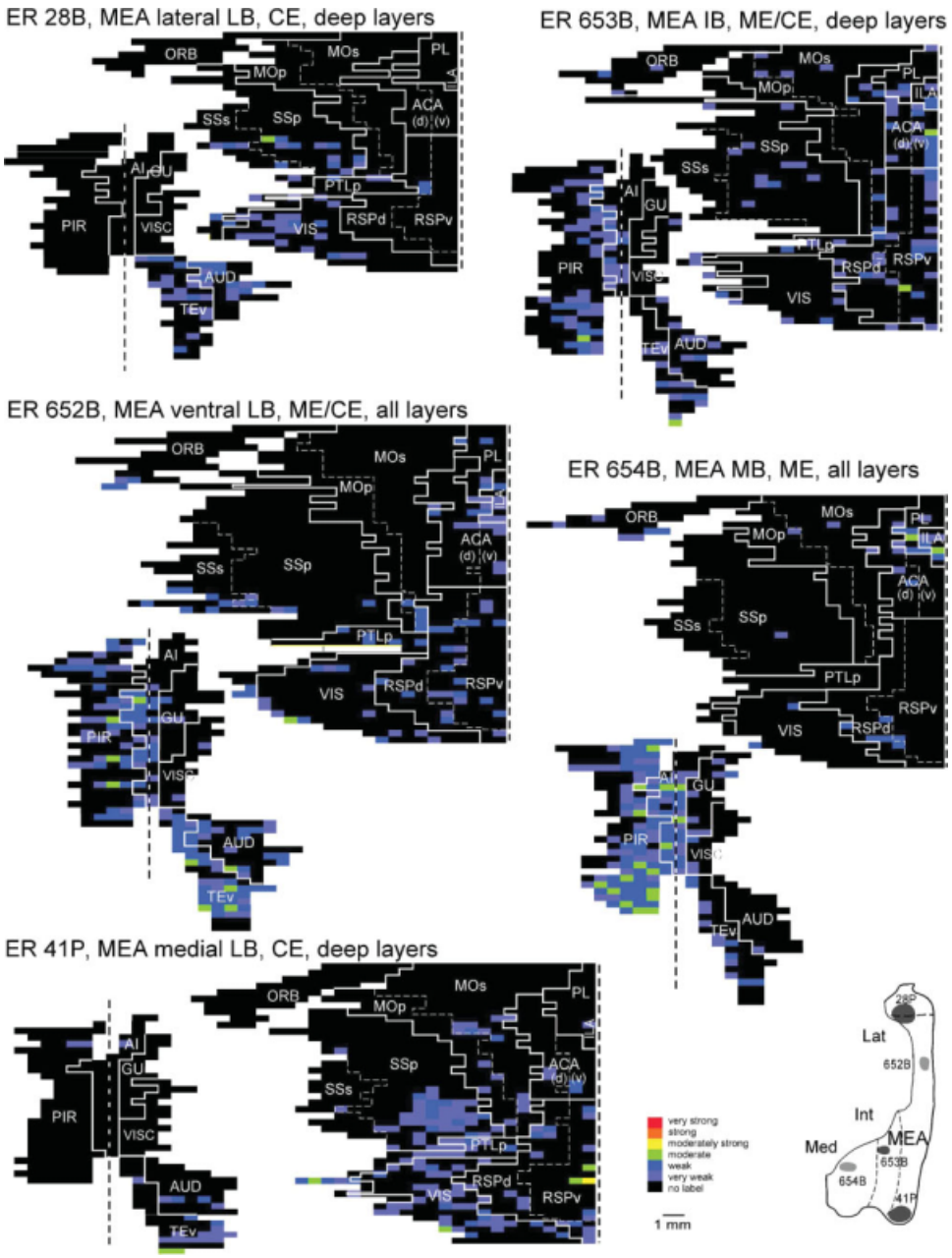

FIGURE 11. Unfolded maps of the neocortical efferents from the medial entorhinal area (MEA). Maps are labeled with the case name, location, band, and layers involved in the injection site (see icon in lower right corner). Voxels in which there was no labeling are black in the figure. Labeling following MEA injections was weak overall, but injections in the lateral band produced the most labeling. The exception was that piriform and insular cortices were most heavily targeted by the medial band. These injections sites involved deep layers or all layers. Thus, the weaker labeling cannot be explained by the laminar location of the injection sites. See list for abbreviations. [Color figure can be viewed in the online issue, which is available at www.interscience.wiley.com.]

(Table 2). LEA and MEA injections, however, tended to produce similar amounts of labeled fibers in temporal areas (Table 3).

LEA and MEA injection sites gave rise to labeling in TEv that was similar in the mean density and total amount of labeling as well as the laminar pattern of labeled terminal fibers. Density of labeled fibers was best described as light. Labeled fibers were observed in layers II–III and V–VI but tended to be heavier in the superficial layers.

LEA injections resulted in a greater density of labeled fibers in auditory regions than did MEA injections sites (Table 2). For the LEA and MEA, injections located in the lateral band provided more input to auditory regions than injection sites located in the intermediate and medial bands (Figs. 10 and 11). For LEA injection sites, there appeared to be a topography such that more rostral sites produced more labeling in auditory regions. Fibers observed in auditory and ventral temporal

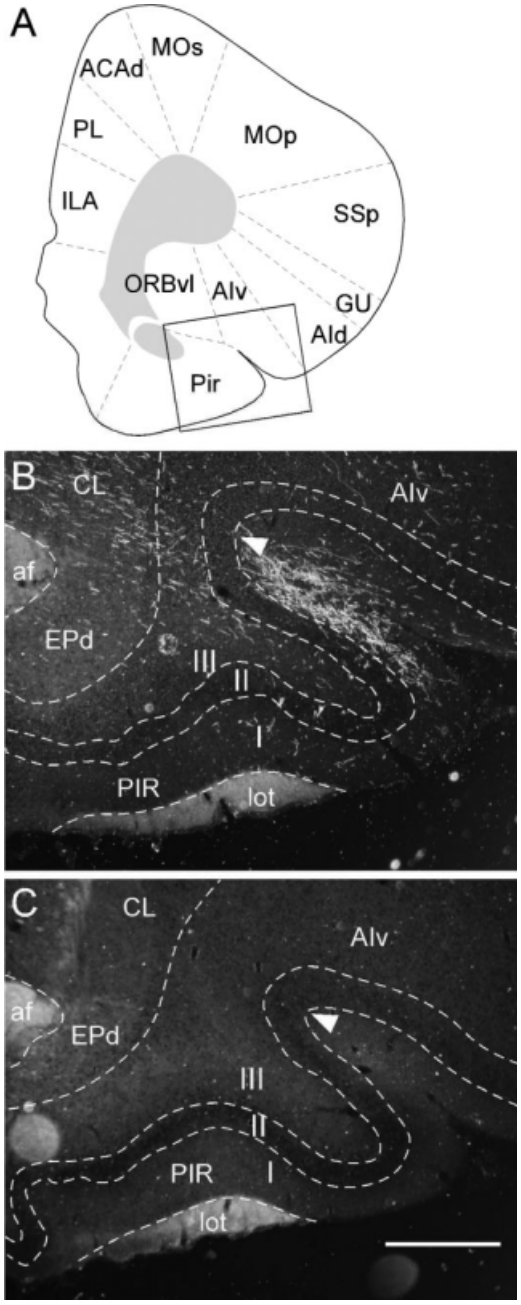

FIGURE 12. Labeling in piriform cortex (PIR) and ventral agranular insular cortex (AIv) following injections in the lateral band of the LEA and MEA. (A) Schematic showing the location of the darkfield photomicrographs. PIR is located below the arrow in both (B) and (C). (B) Labeled fibers resulting from an LEA injection site in the lateral band (case 61B) were heaviest in layer I of PIR near the border with AIv. Weaker labeling was observed in layer III. In general, labeled fibers were restricted to dorsal portions of PIR. Labeling in AIv was moderately dense in layers I and III. (C) In contrast, lateral band injections of the MEA produced few labeled fibers in PIR or insular cortex. No labeled fibers in PIR or AIv were observed following this tracer injection located in the MEA lateral band (case 41P). An injection in the medial MEA band did produce weak fiber labeling. af, anterior forceps of the corpus callosum; CL, claustrum; EPd, dorsal part of the endopiriform nucleus. Scale bar: 250 μm.

regions terminated preferentially in layers I–II, but lighter labeling was observed in deep layers.

Cingulate regions

The LEA and MEA injections resulted in light to very light labeling in cingulate regions. For the LEA injection sites, labeling was light in both anterior cingulate regions (ACAd and ACAv, Table 2), but the amount of labeled fibers was substantially greater in ACAd (Table 3). The majority of the labeled fibers were accounted for by injection sites in the rostral part of the lateral band. In some cases, labeled fibers were observed in all layers, but in other cases labeling was observed in layers I–II and VI, but not layer V. The density of labeled fibers was lighter in the retrosplenial regions and tended to be confined to superficial layers.

For the MEA injection sites, labeling in anterior cingulate and retrosplenial regions was light overall (Table 2), but notably more label was observed in dorsal and ventral retrosplenial cortex (Table 3). The strongest projection appears to originate in the lateral band of the MEA (Fig. 10). Labeled fibers were observed to terminate in layers I–II throughout cingulate regions.

Parietal regions

Density of labeled fibers following injections in the LEA was light in somatosensory regions and very light in the PTLp (Table 2). The largest amount of label was observed in SSp, which is the largest of the parietal regions by area (Table 3). Somatosensory labeling was largely accounted for by an injection in the rostral lateral band of the LEA (Fig. 10). In SSp, labeled fibers were heaviest in layer I. Very light labeling was also observed in layer VI. Labeling in SSs was similar with the exception that layer II was also labeled. Similar to the somatosensory areas, labeling in PTLp was largely accounted for by the rostral lateral band injection site. Labeled fibers were located in layers I and II.

MEA injections gave rise to very light labeling in all parietal regions assessed (Fig. 11 and Table 2). SSp, the largest parietal region, exhibited the largest amount of labeling (Table 3). Every case gave rise to at least some labeling in somatosensory regions, but the most lateral, LB site and the most medial, LB site produced more labeling whereas the ventral sites, one in each band, produced less labeling. Labeled fibers preferentially targeted layer I in SSp and layers I-II in SSs. Labeling in PTLp was very light regardless of the location of the injection site. The injection located in the medial LB produced the most labeled fibers, but the density was still very weak. Labeled fibers were scattered, but could appear in any layer.

Occipital regions

Injections in both the LEA and MEA resulted in only very light labeling in visual regions (Table 2). More labeled fibers were observed in the lateral visual association region, VISl (Table 3). For both the LEA and the MEA, densities of labeled

fibers was heavier following the most lateral and the most medial injections in the lateral band (Figs. 10 and 11). The ventrally located sites produced less labeling in these regions. Labeled fibers were observed in superficial layers I–II, and to a lesser extent, layer VI.

Confirmatory Data Analysis

Cluster analysis was used to examine how anterograde tracer injections placed in PER, POR, LEA, and MEA would be grouped based solely on the density of labeled fibers (Table 2). There was a marked flattening of the *R*-squared curve at the three-cluster solution, indicating that the variance explained by three groups of injection sites would not be substantially improved by an additional division of a group. The three cluster solution is also consistent with a commonly used heuristic method such that the number of clusters is equal to the square root of the number of clustered objects divided by 2 ($k \approx (n/2)^{1/2}$) (Mardia et al., 1979). Figure 13A shows the location of each of the 20 injection sites, color-coded by cluster membership. One of the clusters included all of the POR sites together with the nearby site in caudal area 36, case 27P. Interestingly, the formation of this cluster perfectly reflected neuroanatomical location of the cluster members. PER area 36 case 27P was first joined with the nearby POR 83B. Then POR cases 39P, 134B, and 40R were joined in that order, which also reflects injection site location in the POR. The second cluster included all of the MEA sites, the two nonlateral band LEA sites, and the most caudal area 35 site. The final cluster included the most rostral area 35 sites, all but the most caudal area 36 site, and all three lateral band LEA sites. Notably, had we chosen the two cluster solution, the cluster including all of the POR and the cluster including all of the MEA sites would have been joined in a single cluster.

To determine how cortical efferent data contributed to the grouping of injection sites, the regional patterns of density of labeled terminal fibers were analyzed by multivariate ANOVA (MANOVA). Sixteen of the 26 regional variables were significantly different across clusters at the level of $P < 0.006$. These variables included average density of labeling in PIR, PL, ILA, ORBl, ORBm, ORBvl, AIPd, AIPv, AIPp, GU, VISC, aRSPd, aPTLp, VISl, VISm, and VISp. To illustrate the relationship of significant cortical efferent variables to cluster organization, we conducted a canonical discriminant analysis. To simplify the analysis, related variables were combined: densities for the medial prefrontal regions (PL and ILA, mPFC), the orbital prefrontal regions (ORB), the agranular insular regions (AIP), the granular insular regions (GU and VISC, GI), and the three visual regions (VIS) were averaged. The results of a canonical discriminant analysis of the cluster solution are shown in Figure 13B. The biplot in Figure 13B illustrates the plane of the first two canonical variables identified by the discriminant analysis. These canonical variables represent the linear combinations of the cortical efferent variables. The cortical input variables can be plotted as a vector from the origin to the point described by its canonical coefficients. The vectors show visually that there

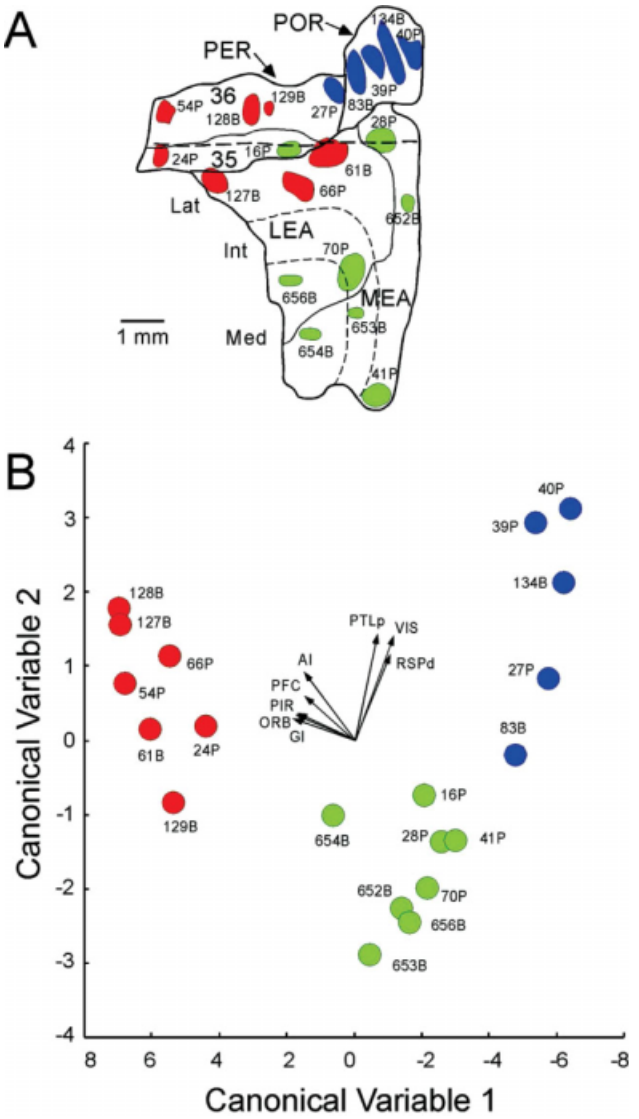

FIGURE 13. Results of cluster and discriminant function analyses of the regional patterns of labeled terminal fibers arising from anterograde tract tracer injections in the perirhinal (PER), postrhinal (POR), lateral entorhinal (LEA), and medial entorhinal (MEA). (A) An unfolded map showing the location of injection sites included in the cluster analysis, color coded by cluster. (B) The cluster analysis yielded three clusters. A canonical discriminant analysis of the cluster solution permitted visualization of the relationship of variables to individual cases. Each experimental case is plotted is placed on the graph according to its score on the first two canonical variables and color coded as in (A). One cluster was dominated by PER and lateral band LEA sites, one was dominated by POR sites, and one was dominated the MEA and remaining LEA sites. The cortical input variables that distinguished the three clusters at the level of $P < 0.006$ are plotted as vectors from the origin. Input variables with similar coordinates were averaged. Because the direction and relative lengths of the vectors are important, the vector lengths were multiplied by a constant (2) to make them more visible. AI, average of AId, AIv, and AIp; GI, average of GU and VISC; ORB, average of ORBl and ORBm; PL/ILA, average of PL and ILA; VIS, average of VISl, VISm, and VISp. [Color figure can be viewed in the online issue, which is available at www.interscience.wiley.com.]

are two sets of vectors that account for much of the variance across clusters. Labeling in piriform, frontal, and insular regions appears to differentiate the PER-LEA lateral band cluster from the POR and MEA clusters, whereas labeling in the retrosplenial, posterior parietal appears to differentiate the PER-LEA and MEA clusters from the POR cluster.

DISCUSSION

This study yielded a number of important findings about parahippocampal connectivity. First, the locations of labeled terminal fibers arising from PER area 35, PER area 36, POR, LEA, and MEA injection sites differed substantially. This was especially evident in the projections to sensory regions (Table 4). Second, aside from the location of labeling, the density and amount of labeled fibers differed substantially depending on the regional location of injection sites. Our findings show that PER area 36 and POR give rise to a greater number of heavy projections, overall, followed by PER area 35 (Fig. 14). A restricted subregion of the LEA also provided substantial cortical efferents, but the evidence suggests that the remainder of LEA and the MEA provide weak efferents to cortical regions. As discussed later, the size of injection sites does not account for these differences in density of labeled fibers. Third, the cortical efferents of each region largely reciprocate the cortical afferents. Fourth, the laminar pattern of terminal fibers supports the conclusion that most of the efferents are feedback projections.

Another contribution of this study is the quantitative nature of the methods of analysis. Because every case included in the study was evaluated using the same quantitative procedures, we were able to exploit exploratory data analysis techniques to provide further insight into our results. The cluster analysis confirmed that anatomical location underlies connectional characteristics of cortical structures. Locations that are near to one another are more likely to exhibit similar connections, but structural boundaries also come into play. For example, a caudal area 36 injection site clustered with the POR sites. This is likely because caudal area 36 has robust connections with visual regions and the POR is largely defined by such connections. On the other hand, the lateral band LEA site, 61B, is quite close to the lateral band MEA site, 28P, yet these sites were in separate clusters. One question worth asking is why the caudal area 35 site, 16P, clustered with the MEA sites. Similar to caudal area 36, caudal area 35 does have more connections with visual and posterior parietal areas. It was the last site to join in the MEA cluster before it merged with the POR cluster. It is also interesting that the LEA lateral band sites clustered with most of the PER sites, in view of the finding that this portion of the LEA provides the most robust cortical efferents of the entorhinal cortex. Another question is why the MEA sites clustered with the sites in the LEA intermediate and medial bands. The analysis suggests that the type of information processed by these areas is similar.

TABLE 4.

Density of Labeled Fibers by Sensory Modality

Efferent regions	Origins				
	Area 36	Area 35	POR	LEA	MEA
Olfactory					
Piriform	94	131	25	188	59
	++	++	+	+++	++
Gustatory					
GU	25	26	4	16	3
	+++	+++	+	++	+
Auditory					
AUD	42	22	45	16	12
	+++	++	+++	++	+
AUDv	30	19	18	6	5
	++++	+++	+++	++	+
Somatosensory					
SS s	49	21	10	25	4
	+++	++	+	++	+
SS p	131	110	55	93	20
	++	++	+	++	+
Visual					
VISl	36	28	106	12	11
	+++	++	+++++	+	+
VISm	7	5	97	4	5
	+	+	++++	+	+
VISp	10	7	78	3	6
	+	+	+++++	+	+

The summed (numbers) and mean (pluses) density of labeled fibers is provided for each modality. Data are selected from Tables 1 and 2.

This is the first study of the cortical efferents of the POR. Using the same cortical boundaries employed in this study, we previously described the cortical afferents of the POR and reported that the strongest afferents arise in VISl, VISm, PTLp, RSPd, and TEv (Burwell and Amaral, 1998a). Very little input arrives from primary visual cortex (VISp). As expected, the cortical efferents of the POR largely reciprocate the cortical afferents. The heaviest labeling was in visual association regions, VISl and VISm, followed by ventral temporal region. Interestingly, the projection to VISp was substantial. This projection has been previously described in the monkey (Rockland and Van Hoesen, 1994; but see Lavenex et al., 2002). The projections to visual regions terminated in deep and superficial layers, consistent with a feedback projection (Felleman and Van Essen, 1991).

We previously showed that the cortical afferents of the PER preferentially target area 36, with the exception of the PIR inputs, which preferentially target area 35 (Burwell and Amaral, 1998a; Burwell, 2001). The heaviest input arises in TEv, but insular and frontal regions also provide input to area 36. In contrast, the input to area 35 is dominated by insular and piriform input. In this study, we report that the PER efferents largely reciprocate the afferents. It should be noted that this is not the first study of PER efferents. McIntyre et al. (McIntyre

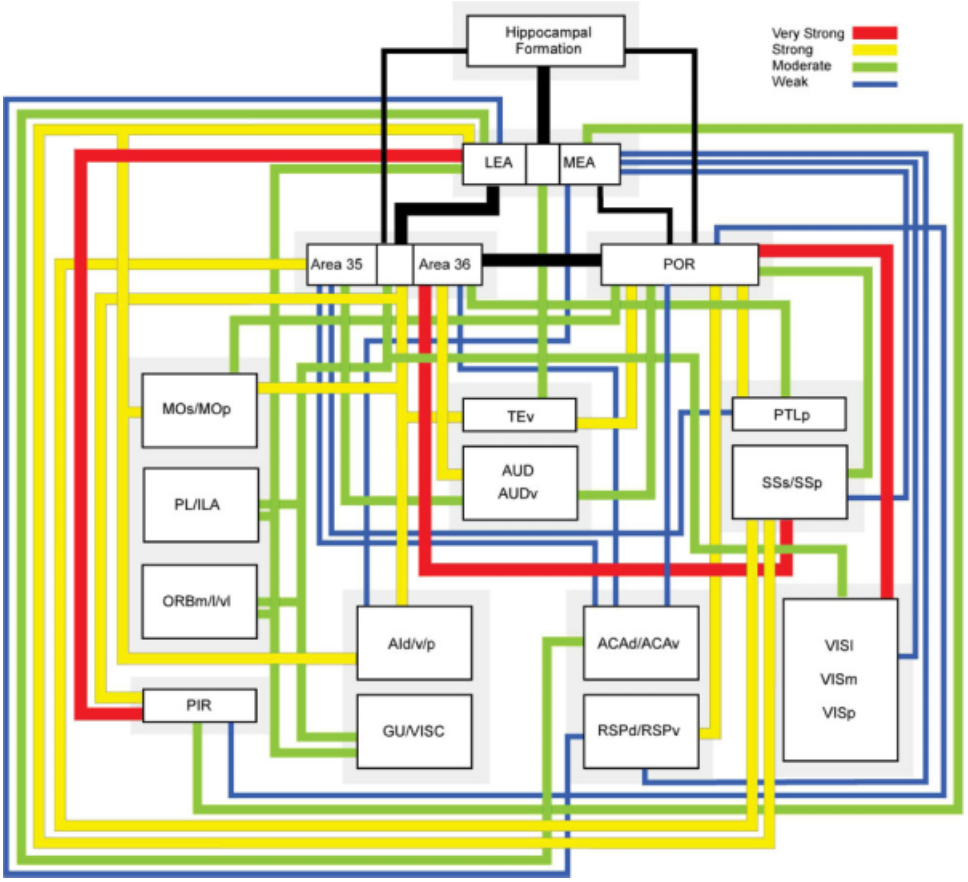

FIGURE 14. Summary of the cortical efferents of the perirhinal, postrhinal, and entorhinal cortices. The wiring diagram was simplified by combining some regions, yielding a total of 65 projections. The relative strength of projections is indicated by color and width of the connection lines. The heaviest 5% are designate very strong (red), the next 25% are strong (yellow), the next 30% are designated moderate (green), the next 15% are designate weak (blue). The bottom 25% of the projections was omitted from the diagram for simplification. The connections shown in black are adapted from other studies. See list for abbreviations. [Color figure can be viewed in the online issue, which is available at www.interscience.wiley.com.]

et al., 1996) examined the efferents of the anterior PER. Other work has addressed these connections in part, for example with frontal regions (Delatour and Witter, 2002), cingulate regions (Jones and Witter, 2007), temporal regions (Room and Groenewegen, 1986; Shi and Cassell, 1997), and occipital regions (Miller and Vogt, 1984). Our study builds on those earlier findings by examining the efferents for all cortical regions for the full rostrocaudal extent of PER and by separately examining the efferents of area 35 or 36.

We confirmed strong projections to motor, orbital, medial, and anterior frontal regions from the PER. Delatour and Witter (2002) also examined parahippocampal projections to frontal regions including medial and orbital prefrontal regions. They compared prefrontal efferents of the PER with those of the neighboring POR and the dorsolateral region of the entorhinal cortex (DLE, Fig. 1C). Consistent with our findings, they reported that the PER and DLE projections terminate primarily in medial prefrontal and agranular insular regions, whereas the POR projections terminate preferentially in ORBvl. We also showed that PER and LEA project to MOs, but POR does not. Though using different nomenclature and borders, Hoover and Vertes (2007) reported that PER areas 35 and 36 and the LEA project to MOs, whereas PER areas 35 and 36, POR and LEA and MEA each project to anterior cingulate cortex, PL, and ILA. PER projections to MOs, ACAd, PL, and ILA were also reported by Conde et al. (1995), though in considerably less detail. These findings are consistent with our own, though we provide more detail with regard to differences in terminal patterns and strength across regions. McIntyre et al. (1996) reported that the anterior PER projects substantially to layers I, II, and VI of FR2 and FR1 (MOs and MOp in our terminology). We observed the same pattern of labeling, but only for the most anterior injection sites in areas 36 and 35. More posterior injections produced weak labeling in MOs and MOp. Furthermore, we found that labeling in those regions following anterior area 35 injections was weaker than that following anterior area 36 injections.

The PER projection to dorsal and posterior portions of agranular insular cortex has been previously observed in both the rat (Saper, 1982; McIntyre et al., 1996) and cat (Witter and Groenewegen, 1986). McIntyre et al. (1996) reported that anterior PER injections of anterograde tracer resulted in strong

labeling in agranular insular cortex. Consistent with our findings, the heaviest labeling was in layers I and II, but layers III–VI were also labeled. Saper (1982) reported that retrogradely labeled cells were more dense in the PER following caudal insular injections. We found, however, that there was evidence for a rostrocaudal topography such that the more rostral PER injections produced more labeling in rostral parts of insular cortex, and vice versa for caudal injections. Consistent with our findings, Delatour and Witter (2002) reported that PER projections to agranular insular regions were similar to those of the DLE. Our data suggests that the DIE projection to agranular insular areas is also similar to that of the DLE. MEA projections to agranular insular regions are relatively weaker, but there are regional differences in the projection. Our data suggests that the MEA projection to agranular insular regions arises entirely from the ME subregion, regardless of the band of origin.

Given the PER contribution to stimulus perception and memory as well as cross-modal processing, the PER projections to sensory regions are of interest. Others have suggested that the rostral part of PER is dominated by somatosensory input (Shi and Cassell, 1998a,b). We previously showed, however, that all parts of the PER, including the rostral PER, receive input from all sensory modalities (Burwell, 2001). The termination of sensory inputs does, however, show a distinct topography. Anterior area 36 receives more input from somatosensory regions, mid-rostrocaudal area 36 receives more input from auditory regions, caudal area 36 receives more input from visual regions, and area 35 receives more input from PIR (Burwell, 2001). We also showed that sensory input arises preferentially from secondary associational regions (Burwell and Amaral, 1998a).

This study demonstrates that the PER projects back to all sensory regions (Table 4), and that the cortical efferents show topographies similar to those of the cortical afferents with respect to sensory modality. We and others have shown that the PER receives input from PIR (Luskin and Price, 1983; Burwell and Amaral, 1998a; Schwabe et al., 2004). Here, we described the topography of the reciprocal projection. Consistent with prior findings (Haberly, 2001), we found that, overall, the PER projects more heavily to posterior PIR than anterior PIR. We further showed that the projections arising from both areas 35 and 36 show different terminal patterns. There is evidence for a rostrocaudal topography for the area 36 projection. In contrast, for the area 35 projection there is a rostrocaudal difference in strength, but not pattern. The reciprocal connections between PER and PIR support the notion that PIR is more similar to sensory associational cortex than primary sensory cortex (Johnson et al., 2000).

Regarding connections with visual regions, Miller and Vogt (1984) reported that perirhinal cortex has modest connections with primary and secondary visual regions, and that the visual input to perirhinal cortex is stronger than the return projection. Our data further reveal that the connections with secondary visual regions are more robust than those with primary visual cortex (present paper and Burwell and Amaral, 1998a). Though there is a modest projection to visual regions arising in the PER, the POR connections with visual regions are substantially more robust.

Swanson and Kohler (1986) reported sometime ago that the EC of the rat projects to "the entire cortical mantle." Their injection sites, however, were restricted to the strip of LEA adjacent to the PER and POR. Insausti et al. (1997) examined the cortical efferents of the entire EC and reported that, similar to the monkey, most of the EC does not project strongly to the cortex. Rather, all cortical regions receive input from EC, but from a small complement of cells. They provided evidence that widespread projections originate in the deep layers of the strip of entorhinal cortex adjacent to the PER and POR including DLE and the laterodorsal CE (Fig. 1C). Our findings confirm that the EC projects broadly to cortical regions. In contrast to the earlier studies, however, we found that all parts of the EC provided widespread projections to cortical regions, but that there were substantial regional differences in the strength of the projections. Our data indicate that the DLE, which largely coincides with the lateral band of the LEA, gives rise to strong and widespread cortical efferents, but that all other regions of the EC give rise to distributed, but weak cortical efferents. Our case 28B, located in deep layers of the laterodorsal CE, produced relatively weak labeling in cortical regions. Though the injection site was largely in deep layers, there was involvement of layer III, so we could use the labeling in CA1 as an indicator of transport. Labeling in CA1 was very strong, suggesting that transport was good. Taken together, the evidence suggests that only the DLE provides strong and widespread projections to the cortical mantle.

With the exception of the PIR projection and possibly the cortical efferents arising in rostral DLE, the EC projections are not as strong as those of the PER and POR. Within the EC, the LEA projections are more robust than those of the MEA. Swanson and Kohler (1986) reported that the densest cortical projection from LEA targeted medial prefrontal regions. Our data indicate that the densest cortical projections target the piriform and agranular insular regions; the medial prefrontal projections arising in LEA, however, are stronger than the other frontal projections.

Insausti et al. (1997) provided evidence that MEA gave rise to more substantial projections to cortical regions than we report here. Specifically, there was evidence for a dense projection to the retrosplenial cortex arising from deep layers of dorsocaudal MEA in area CE. The evidence was based on a very large anterograde tracer injection involving layers III–VI. A nearby injection involving only superficial layers did not result in retrosplenial labeling. In our study, there was evidence for a light projection to retrosplenial cortex, as compared to retrosplenial projections arising in, for example, the POR. This conclusion is based on a much smaller injection site located in the same place and involving both superficial and deep layers (MEA 28P). The injection sites in our study were all relatively small, although transport was similar across cases. Thus, it may be that the MEA projections to cortical regions are somewhat underestimated in the present paper. It should be noted,

however, that there was good transport in all MEA injections. In addition, all injections involved at least layer III and produced dense labeling in the hippocampus. Finally, the amount of labeling as indicated in the unfolded maps is not related to injection site size. For example, the smallest PER injection (129B) gave rise to the next largest amount of labeling arising from a PER injection; and the largest POR site (134B) gave rise to modest amounts of labeled fibers.

Alternatively, the meager connections of the MEA may reflect an often-noted principle of corticocortical connections, i.e., regions that are in closer proximity are more strongly interconnected. Thus, the MEA, which is structurally isolated from neocortex, is less heavily connected. The connections of other regions examined also reflect this principle of connectivity in the topography of connections. For example, efferents arising from rostral 35 and 36 terminate preferentially in rostral cortical regions, such as frontal and insular areas; whereas projections originating from caudal portions of the PER have heavier terminations in caudal cortical regions such as parietal and occipital areas. Similarly, the POR, which is situated at the caudal pole, provides meager input to frontal, insular, anterior cingulate, and somatosensory regions, and projects more strongly to the more proximal parietal, retrosplenial, and occipital areas.

The exclusion of the olfactory bulb from analysis is a limitation of the this study of the cortical efferents of the PER, POR, and EC as well as our earlier study of the cortical afferents of the same regions (Burwell and Amaral, 1998a). Fortunately, others have documented those connections. It is well established that the olfactory bulb projects to the lateral and medial entorhinal areas (e.g., Kosel et al., 1981). Kosel et al. (1981) also showed that the adjacent PER and POR do not receive olfactory bulb input. Regarding a cortical projection to the olfactory bulb, there is some evidence that the lateral entorhinal area provides a small input (de Olmos et al., 1978). The location of the origin of the projection appears to be in entorhinal field VIE as defined by Insausti et al. (1997). To our knowledge, there is no evidence for PER or POR projections directly to the olfactory bulb.

Although we did not include the olfactory bulb, we did characterize the parahippocampal connections with PIR. These connections are of interest because these regions are involved in limbic kindling of seizures (McIntyre and Kelly, 2000). The strong connectivity between the EC and olfactory cortex has been well documented (Witter and Groenewegen, 1986; Witter et al., 1989a; Insausti et al., 1997). Insausti (1997) reported that the projections to PIR originate in all entorhinal subdivisions, but preferentially arise in DIE, VIE, and ME (Fig. 1C). Our findings suggest, however, that the PIR projection arises preferentially in DLE and ME. We found that the LEA provides the heaviest projection to PIR followed by the PER and the MEA.

Prior work has shown that layer II of PIR gives rise to a prominent projection to the LEA (Powell et al., 1965; Beckstead, 1978; Haberly and Price, 1978; Burwell and Amaral, 1998a). Here, we showed that the LEA return projections terminate mainly in deep layer I, and to a lesser extent in III. We also showed that the LEA projection is stronger than the MEA projection. Similar to the findings of Insausti et al. (1997), we found that the rostral DLE provides substantial input to the molecular layer of PIR, but we found that caudal DLE also provided input. The differences cannot be explained by laminar differences in the location of label. Regarding the MEA projection, Insausti et al. (1997) showed heavier density of labeled fibers arising from mid-mediolateral levels of CE than we did, but the injection sites analyzed were substantially larger than any of our injection sites. We found evidence for a projection from all parts of the MEA except the medial and lateral extremes of CE, which were not sampled by the Insausti et al. (1997).

There are substantial differences across the PER, POR, and EC in the efferents to sensory regions. Area 36 targets multiple sensory regions including piriform, gustatory, somatosensory, auditory, and visual regions (Table 4). In contrast, the POR efferents preferentially target visual regions, though auditory regions are also targeted. Entorhinal cortex projects to sensory regions as well. The strength, however, is modest compared to the sensory efferents of the PER and POR. Some of the sensory projections arising in the EC have been previously reported, for example to the visual cortex (Insausti et al., 1997) and to the auditory cortex (Kosel et al., 1982). Our data indicate, however, that the efferents to visual regions are very weak, and that the weak projections to auditory regions arise in the LEA.

Reciprocity

Our earlier study of the cortical afferents of the PER, POR, and EC used the same regional borders and nomenclature used here (Burwell and Amaral, 1998a), making it possible to assess the reciprocity of the cortical efferents and afferents of these regions. Overall, there is considerable reciprocity in the cortical connections of the PER, POR, and EC. There are, however, regional differences. In general, the cortical connections of the PER and POR show more reciprocity than those of the EC. For the LEA some connections are reciprocal and others are not. MEA connections tend to be weakly reciprocal.

The PER cortical efferents are strongly reciprocated for the most part. PIR afferent projections to area 36 arise from caudal PIR and terminate in superficial layers. The return projection from area 36 also targets the caudal PIR. The situation is more complex for area 35. PIR afferents to area 35 arise from rostral portions of PIR and terminate preferentially in rostral area 35. The return projection arises at all levels of area 35 and terminates in all levels of PIR. The rostral efferents, however, are stronger.

Analysis of frontal afferents to the PER shows that orbital and infralimbic areas provide the strongest input to areas 35 and 36 of PER. Return projections from PER to frontal regions are also stronger in these areas. Agranular insular regions project to areas 35 and 36; however return projections are not fully reciprocal. Area 36 is innervated primarily by ventral agranular insular regions, while its efferents terminate predominantly in dorsal and posterior agranular insular regions.

Area 35 is reciprocally connected with posterior agranular insular regions. Auditory regions target rostral area 36 and provide strong input to area 35. Area 36 returns a moderate projection to dorsal auditory regions; return projections from area 35 are also moderate. Ventral temporal regions are reciprocally connected with area 36; area 35 receives a stronger projection from ventral temporal regions than it returns. Caudal portions of parietal regions innervate area 36; similarly area 36 efferents terminate preferentially in caudal parietal areas. Area 35 is reciprocally connected with parietal cortex along the rostrocaudal extent of the region. Finally, visual association regions weakly innervate area 36, and area 36 returns a moderate projection to lateral visual association regions.

Postrhinal cortical connections are all reciprocal. The PIR projects weakly to POR; similarly POR efferents to PIR are minimal. Frontal and insular regions also project weakly to POR and receive weak return projections. Within parietal regions, auditory areas project weakly to POR, whereas ventral temporal regions project strongly to POR. Postrhinal efferents to auditory regions are moderate; in contrast a heavy projection to ventral temporal areas arises from POR (Fig. 7). Dorsal retrosplenial cortex provides the majority of the cingulate region input to POR; return projections also target dorsal retrosplenial regions. Both posterior parietal and visual association regions are strongly and reciprocally connected with POR.

There is some reciprocity in the cortical connections of the EC. For the LEA, the PIR and agranular insular connections are reciprocal. In addition, the LEA provides output to MOs and SSp that is not reciprocal. The MEA receives less direct cortical input than the LEA. PIR, ventral temporal, retrosplenial, and visual association areas directly innervate the MEA. Although all cortical projections arising from the MEA are weak; the projections to PIR and ventral temporal association cortex appear relatively stronger (Fig. 11). With the exception of the PIR, strongest outputs of the LEA and the MEA target the PER and the POR (Burwell and Amaral, 1998a,b)

Functional Implications

Our interest in the cortical efferents of the PER, POR, and EC arises from their known contributions to memory. We do not intend, however, to suggest that the corticocortical connections are the only ones to support memory function. Clearly the connections with subcortical structures and circuits are important for memory processes (Aggleton et al., 1995; Campeau and Davis, 1995; Winters and Bussey, 2005a). Indeed, it is clear that these regions also receive different subcortical inputs (Agster, 2007; Furtak et al., 2007; Kerr et al., 2007). Our focus in this study, however, is the sensory and associational connections of these parahippocampal structures.

We and others have suggested that cortical input to the hippocampus is processed through two parallel streams (Burwell, 2000; Lavenex and Amaral, 2000; Witter et al., 2000). One stream incorporates the PER and the LEA, and is specialized for processing nonspatial information about discrete stimuli, for example objects, odors, or auditory stimuli. The other stream incorporates the POR and the MEA and is specialized for processing information about spatial location or spatial context. This study provides evidence that the functional specialization of the cortical components of these two processing streams is bi-directional. However, the exploratory analysis suggests that the segregation of spatial and nonspatial information may be less segregated in the return projections.

The degree to which the two processing streams are segregated is an important question. Jones and Witter (2007) recently provided evidence that integration occurs at the level of the cingulate cortices in a network that includes prelimbic/infralimbic, anterior cingulate, and retrosplenial cortices. They reported that rostral cingulate regions (infralimbic/prelimbic cortices) primarily connect with PER and LEA, and the caudal cingulate regions (retrosplenial cortex) primarily connect with POR and MEA. The mid-rostrocaudal region (cingulate areas) has connections with both processing streams, suggesting that the mid-rostrocaudal cingulate area may provide the circuitry for integration of information across the two processing streams. In this study, we showed that the PER and LEA project most strongly to the infralimbic and prelimbic cortices, whereas the POR and MEA project more strongly to the retrosplenial regions. The input to ACAd is equally strong from all projection regions (with the exception of MEA which has weak efferents overall). Rostral cingulate regions have been functionally dissociated from caudal ones. The rostrally located prelimbic/infralimbic cortex contributes to attentional processing of discrete stimuli (Chudasama and Muir, 2001; Chudasama et al., 2003; Chudasama and Robbins, 2003); whereas the caudally located retrosplenial cortex has been implicated in spatial functions (Cooper and Mizumori, 2001; Cain et al., 2006).

Integration also occurs at the level of the PER and POR. The POR provides a heavy input to the PER, but the reciprocal connections are relatively weak (Burwell and Amaral, 1998b). The situation is similar in the monkey (Suzuki and Amaral, 1994). The anatomy suggests that the POR may inform the PER about the context in which discrete stimuli are located. This notion is consistent with human imaging data. Buffalo et al. (2006) reported that the PER was active during both spatial and object memory encoding. In contrast, the anterior parahippocampal cortex (the primate POR homolog) was active only during spatial encoding. One interpretation is that the object processing functions of the PER are modulated by POR input. Indeed, Pihlajamaki et al. (2004) reported that the PER and the anterior parahippocampal cortex were more active relative to baseline when a novel object was presented in an array of familiar objects. In contrast, the posterior parahippocampal cortex was activated when familiar objects were presented in novel spatial arrangements.

A third level at which information may be integrated across the two processing streams is in the EC. The DG-projecting bands are defined by patterns of intrinsic connectivity such that a tract tracer injection will result in labeling in the band of origin regardless of region, i.e., the labeling will span the LEA and the MEA for that band. We have shown that the DG-projecting bands of the EC have different cortical inputs (Burwell

and Amaral, 1998a). This study reveals that the DG-projecting bands of the EC also display unique patterns of cortical outputs. The lateral band of the LEA (largely overlapping with the DLE subregion) provides the strongest and most extensive output to cortical structures. Fiber labeling from this region is strongest within PIR, insular and anterior cingulate regions (Fig. 10). Relatively weak output arises from the lateral band of the MEA, but the majority of labeled fibers from this area are observed to terminate in retrosplenial and occipital regions (Fig. 11). Efferent projections from the intermediate bands of both the LEA and MEA are very light. The medial bands of the LEA and MEA provide weak input to the PIR and insular regions. Finally, the pattern of labeled fibers within the PIR following tracer injections to the LEA and MEA is unique. The lateral band of the LEA provides strong projections to the PIR, while efferent projections from the medial band of the LEA are more modest. Conversely, the medial band of the MEA provides stronger innervation of the PIR as compared to the lateral band.

Prior research has shown that the spatial and nonspatial input to the hippocampus via the EC is somewhat segregated into two processing streams. As discussed above, the two processing streams are connected at multiple hierarchical levels. We have shown that the cortical efferents of these regions largely reciprocate the cortical afferents such that spatial and nonspatial output is also segregated. Thus, it appears that spatial and nonspatial information may be integrated on the output side of the hippocampus as well as the input side.

CONCLUSIONS

We have analyzed the cortical output of the PER, POR, and EC. Our findings indicate that the cortical efferents of these regions are differ in both strength and target.The strongest efferents arise in PER area 36 and the POR. Projections from PER area 35 and entorhinal LEA are weaker. Output from the MEA is even weaker in comparison. Although the EC, especially the MEA, provides limited output to the regions analyzed in this study, both the LEA and the MEA are heavily interconnected with the PER and POR (Burwell and Amaral, 1998b), which do project strongly to neocortex. Thus, this study confirms that the major route for hippocampal output to higher order cortical regions is via the entorhinal connections with the PER and the POR.

REFERENCES

Aggleton JP, Neave N, Nagle S, Hunt PR. 1995. A comparison of the effects of anterior thalamic, mamillary body and fornix lesions on reinforced spatial alternation. Behav Brain Res 68:91–101.

Agster KL. 2007. Structure and Function of the Rodent Postrhinal Cortex: Comparisons to Other Cortical Regions [Doctoral]. Providence, RI: Brown University. 317p.

Arnault P, Roger M. 1990. Ventral temporal cortex in the rat: Connections of secondary auditory areas Te2 and Te3. J Comp Neurol 302:110–123.

Beckstead RM. 1978. Afferent connections of the entorhinal area in the rat as demonstrated by retrograde cell-labeling with horseradish peroxidase. Brain Res 152:249–264.

Bucci DJ, Burwell RD. 2004. Deficits in attentional orienting following damage to the perirhinal or postrhinal cortices. Behav Neurosci 118:1117–1122.

Bucci DJ, Phillips RG, Burwell RD. 2000. Contributions of postrhinal and perirhinal cortex to contextual information processing. Behav Neurosci 114:882–894.

Bucci DJ, Saddoris MP, Burwell RD. 2002. Contextual fear discrimination is impaired by damage to postrhinal or perirhinal cortex. Behav Neurosci 116:479–488.

Buffalo EA, Bellgowan PS, Martin A. 2006. Distinct roles for medial temporal lobe structures in memory for objects and their locations. Learn Mem 13:638–643.

Burwell RD. 2000. The parahippocampal region: Corticocortical connectivity. Ann N Y Acad Sci 911:25–42.

Burwell RD. 2001. The perirhinal and postrhinal cortices of the rat: Borders and cytoarchitecture. J Comp Neurol 437:17–41.

Burwell RD, Amaral DG. 1998a. Cortical afferents of the perirhinal, postrhinal, and entorhinal cortices. J Comp Neurol 398:179–205.

Burwell RD, Amaral DG. 1998b. Perirhinal and postrhinal cortices of the rat: Interconnectivity and connections with the entorhinal cortex. J Comp Neurol 391:293–321.

Burwell RD, Bucci DJ, Sanborn MR, Jutras MJ. 2004a. Postrhinal and perirhinal contributions to remote memory for context. J Neurosci 24:11023–11028.

Burwell RD, Saddoris MP, Bucci DJ, Wiig KA. 2004b. Corticohippocampal contributions to spatial and contextual learning. J Neurosci 24:3826–3836.

Bussey TJ, Saksida LM, Murray EA. 2003. Impairments in visual discrimination after perirhinal cortex lesions: Testing 'declarative' vs. 'perceptual-mnemonic' views of perirhinal cortex function. Eur J Neurosci 17:649–660.

Cain DP, Humpartzoomian R, Boon F. 2006. Retrosplenial cortex lesions impair water maze strategies learning or spatial place learning depending on prior experience of the rat. Behav Brain Res 170:316–325.

Campeau S, Davis M. 1995. Involvement of subcortical and cortical afferents to the lateral nucleus of the amygdala in fear conditioning measured with fear-potentiated startle in rats trained concurrently with auditory and visual conditoned stimuli. J Neurosci 15:2312–2327.

Campolattaro MM, Freeman JH. 2006a. Perirhinal cortex lesions impair feature-negative discrimination. Neurobiol Learn Mem 86:205–213.

Campolattaro MM, Freeman JH. 2006b. Perirhinal cortex lesions impair simultaneous but not serial feature-positive discrimination learning. Behav Neurosci 120:970–975.

Chapin JK, Lin CS. 1984. Mapping the body representation in the SI cortex of anesthetized and awake rats. J Comp Neurol 229:199–213.

Chudasama Y, Muir JL. 2001. Visual attention in the rat: A role for the prelimbic cortex and thalamic nuclei? Behav Neurosci 115:417–428.

Chudasama Y, Robbins TW. 2003. Dissociable contributions of the orbitofrontal and infralimbic cortex to pavlovian autoshaping and discrimination reversal learning: Further evidence for the functional heterogeneity of the rodent frontal cortex. J Neurosci 23:8771–8780.

Chudasama Y, Baunez C, Robbins TW. 2003. Functional disconnection of the medial prefrontal cortex and subthalamic nucleus in attentional performance: Evidence for corticosubthalamic interaction. J Neurosci 23:5477–5485.

Conde F, Maire-Lepoivre E, Audinat E, Crepel F. 1995. Afferent connections of the medial frontal cortex of the rat. II. Cortical and subcortical afferents. J CompNeurol 352:567–593.

Cooper BG, Mizumori SJ. 2001. Temporary inactivation of the retrosplenial cortex causes a transient reorganization of spatial coding in the hippocampus. J Neurosci 21:3986–4001.

de Olmos J, Hardy H, Heimer L. 1978. The afferent connections of the main and the accessory olfactory bulb formations in the rat: An experimental HRP-study. J Comp Neurol 181:213–244.

Deacon TW, Eichenbaum H, Rosenberg P, Eckmann KW. 1983. Afferent connections of the perirhinal cortex in the rat. J Comp Neurol 220:168–190.

Delatour B, Witter MP. 2002. Projections from the parahippocampal region to the prefrontal cortex n the rat: Evidence of multiple pathways. Eur J Neurosci 15:1400–1407.

Dolorfo CL, Amaral DG. 1998a. Entorhinal cortex of the rat: Organization of intrinsic connections. J Comp Neurol 398:49–82.

Dolorfo CL, Amaral DG. 1998b. The entorhinal cortex of the rat: Topographic organization of the cells of origin of the perforant path projection to the dentate gyrus. J Comp Neurol 398:25–48.

Donoghue JP, Wise SP. 1982. The motor cortex of the rat: Cytoarchitecture and microstimulation mapping. J Comp Neurol 212:76–88.

Eacott MJ, Gaffan EA. 2005. The roles of perirhinal cortex, postrhinal cortex, and the fornix in memory for objects, contexts, and events in the rat. Q J Exp Psychol B 58:202–217.

Eacott MJ, Norman G, Gaffan EA. 2003. The role of perirhinal cortex in visual discrimination learning for visual secondary reinforcement in rats. Behav Neurosci 117:1318–1325.

Egorov AV, Hamam BN, Fransen E, Hasselmo ME, Alonso AA. 2002. Graded persistent activity in entorhinal cortex neurons. Nature 420:173–178.

Ennaceur A, Aggleton JP. 1997. The effects of neurotoxic lesions of the perirhinal cortex combined to fornix transection on object recognition memory in the rat. Behav Brain Res 88:181–193.

Felleman DJ, Van Essen DC. 1991. Distributed hierarchical processing in the primate cerebral cortex. Cerebral Cortex 1:1–47.

Furtak SC, Wei SM, Agster KL, Burwell RD. 2007. Functional neuroanatomy of the parahippocampal region: Perirhinal and postrhinal cortices. Hippocampus 17:709–727.

Fyhn M, Molden S, Witter MP, Moser EI, Moser MB. 2004. Spatial representation in the entorhinal cortex. Science 305:1258–1264.

Gerfen CR, Sawchenko PE. 1984. An anterograde neuroanatomical tracing method that shows the detailed morphology of neurons, their axons and terminals: Immunohistochemical localization of an axonally transported plant lectin, *Phaseolus vulgaris*-Leucoagglutinin (PHA-L). Brain Res 290:219–238.

Gordon AD. 1999. Classification. In: Classification. Cox DR, Isham V, Keiding N, Reid N, Tong H, Louis T, editors. London: Chapman & Hall/CRC. 256p.

Haberly LB. 2001. Parallel-distributed processing in olfactory cortex: New insights from morphological and physiological analysis of neuronal circuitry. Chem Senses 26:551–576.

Haberly LB, Price JL. 1978. Association and commissural fiber systems of the olfactory cortex in the rat. I. Systems originating in the piriform cortex and adjacent areas. J Comp Neurol 178:711–740.

Hafting T, Fyhn M, Molden S, Moser MB, Moser EI. 2005. Microstructure of a spatial map in the entorhinal cortex. Nature 436:801–806.

Hoover WB, Vertes RP. 2007. Anatomical analysis of afferent projections to the medial prefrontal cortex in the rat. Brain Struct Funct 212:149–179.

Insausti R, Amaral DG, Cowan MW. 1987. The entorhinal cortex of the monkey. II. Cortical afferents. J CompNeurol 264:356–395.

Insausti R, Herrero MT, Witter MP. 1997. Entorhinal cortex of the rat: Cytoarchitectonic subdivisions and the origin and distribution of cortical efferents. Hippocampus 7:146–183.

Jarrard LE, Davidson TL, Bowring B. 2004. Functional differentiation within the medial temporal lobe in the rat. Hippocampus 14:434–449.

Johnson DM, Illig KR, Behan M, Haberly LB. 2000. New features of connectivity in piriform cortex visualized by intracellular injection of pyramidal cells suggest that "primary" olfactory cortex functions like "association" cortex in other sensory systems. J Neurosci 20:6974–6982.

Jones BF, Witter MP. 2007. Cingulate cortex projections to the parahippocampal region and hippocampal formation in the rat. Hippocampus 17:957–976.

Kerr KM, Agster KL, Furtak SC, Burwell RD. 2007. Functional neuroanatomy of the parahippocampal region: The lateral and medial entorhinal areas. Hippocampus 17:697–708.

Kosel KC, Van Hoesen GW, West JR. 1981. Olfactory bulb projections to the parahippocampal area of the rat. J Comp Neurol 198:467–482.

Kosel KC, Van Hoesen GW, Rosene DL. 1982. Non-hippocampal cortical projections from the entorhinal cortex in the rat and rhesus monkey. Brain Res 244:201–213.

Krettek JE, Price JL. 1977. The cortical projections of the mediodorsal nucleus and adjacent thalamic nuclei in the rat. J Comp Neurol 171:157–192.

Krieg WJS. 1946. Connections of the cerebral cortex. I. The albino rat A Topography of the cortical areas. J CompNeurol 84:221–275.

Lavenex P, Amaral DG. 2000. Hippocampal-neocortical interaction: A hierarchy of associativity. Hippocampus 10:420–430.

Lavenex P, Suzuki WA, Amaral DG. 2002. Perirhinal and parahippocampal cortices of the macaque monkey: Projections to the neocortex. J Comp Neurol 447:394–420.

Lipton PA, White JA, Eichenbaum H. 2007. Disambiguation of overlapping experiences by neurons in the medial entorhinal cortex. J Neurosci 27:5787–5795.

Luskin MB, Price JL. 1983. The topographic organization of associational fibers of the olfactory system in the rat, including centrifugal fibers to the olfactory bulb. J Comp Neurol 216:264–291.

Malkova L, Mishkin M. 2003. One-trial memory for object-place associations after separate lesions of hippocampus and posterior parahippocampal region in the monkey. J Neurosci 23:1956–1965.

Mardia KV, Kent JT, Bibby JM. 1979. Multivariate Analysis. San Diego: Academic Press.

Mascagni F, McDonald AJ, Coleman JR. 1993. Corticoamygdaloid and corticocortical projections of the rat temporal cortex: A *Phaseolus vulgaris* Leucoagglutinin study. Neuroscience 57:697–715.

McGaughy J, Koene RA, Eichenbaum H, Hasselmo ME. 2005. Cholinergic deafferentation of the entorhinal cortex in rats impairs encoding of novel but not familiar stimuli in a delayed nonmatch-to-sample task. J Neurosci 25:10273–10281.

McIntyre DC, Kelly ME. 2000. The parahippocampal cortices and kindling. Ann N Y Acad Sci 911:343–354.

McIntyre DC, Kelly ME, Staines WA. 1996. Efferent projections of the anterior perirhinal cortex in the rat. J Comp Neurol 369:302–318.

Miller MW, Vogt BA. 1984. Direct connections of rat visual cortex with sensory, motor, and association cortices. J Comp Neurol 226:184–202.

Norman G, Eacott MJ. 2005. Dissociable effects of lesions to the perirhinal cortex and the postrhinal cortex on memory for context and objects in rats. Behav Neurosci 119:557–566.

Paxinos G, Watson C. 1998. The Rat Brain in Stereotaxic Coordinates. San Diego: Academic Press.

Pihlajamaki M, Tanila H, Kononen M, Hanninen T, Hamalainen A, Soininen H, Aronen HJ. 2004. Visual presentation of novel objects and new spatial arrangements of objects differentially activates the medial temporal lobe subareas in humans. Eur J Neurosci 19: 1939–1949.

Powell TPS, Cowan MM, Raisman G. 1965. The central olfactory connexions. J Anat 99:791–813.
Rockland KS, Van Hoesen GW. 1994. Direct temporal-occipital feedback connections to striate cortex (V1) in the macaque monkey. Cereb Cortex 4:300–313.
Room P, Groenewegen HJ. 1986. Connections of the parahippocampal cortex. I. Cortical afferents. J Comp Neurol 251:415–450.
Rose M. 1929. Cytoarchitektonischer atlas der Groshirnrinde der Maus. Journal Fur Psychologie und Neurologie 40:1–32.
Saper CB. 1982. Convergence of autonomic and limbic connections in the insular cortex of the rat. J Comp Neurol 210:163–173.
Schwabe K, Ebert U, Loscher W. 2004. The central piriform cortex: Anatomical connections and anticonvulsant effect of GABA elevation in the kindling model. Neuroscience 126:727–741.
Shi CJ, Cassell MD. 1997. Cortical, thalamic, and amygdaloid projections of rat temporal cortex. J Comp Neurol 382:153–175.
Shi CJ, Cassell MD. 1998a. Cascade projections from somatosensory cortex to the rat basolateral amygdala via the parietal insular cortex. J Comp Neurol 399:469–491.
Shi CJ, Cassell MD. 1998b. Cortical, thalamic, and amygdaloid connections of the anterior and posterior insular cortices. J Comp Neurol 399:440–468.
Suzuki WA, Amaral DG. 1994. Topographic organization of the reciprocal connections between the monkey entorhinal cortex and the perirhinal and parahippocampal cortices. J Neurosci 14:1856–1877.
Swanson LW. 1992. Brain Maps: Structure of the Rat Brain. Amsterdam: Elsevier.
Swanson LW, Kohler C. 1986. Anatomical evidence for direct projections from the entorhinal area to the entire cortical mantle in the rat. J Neurosci 6:3010–3023.
Van Hoesen GW, Pandya DN, Butters N. 1972. Cortical afferents to the entorhinal cortex of the Rhesus monkey. Science 175:1471–1473.
Veenman CL, Reiner A, Honig MG. 1992. Biotinylated dextran amine as an anterograde tracer for single- and double-labeling studies. J Neurosci Methods 41:239–254.
Vogt BA, Miller MW. 1983. Cortical connections between rat cingulate cortex and visual, motor, and postsubicular cortices. J Comp Neurol 216:192–210.
Wiig KA, Cooper LN, Bear MF. 1996. Temporally graded retrograde amnesia following separate and combined lesions of the perirhinal cortex and fornix in the rat. Learn Mem 3:313–325.
Winters BD, Bussey TJ. 2005a. Removal of cholinergic input to perirhinal cortex disrupts object recognition but not spatial working memory in the rat. Eur J Neurosci 21:2263–2270.
Winters BD, Bussey TJ. 2005b. Transient inactivation of perirhinal cortex disrupts encoding, retrieval, and consolidation of object recognition memory. J Neurosci 25:52–61.
Witter MP. 1989. Connectivity of the rat hippocampus. In: Chan-Palay V, Kohler C, editors. The Hippocampus—New Vistas. New York: Alan Liss. pp 53–69.
Witter MP, Groenewegen HJ. 1986. Connections of the parahippocampal cortex in the cat. III. Cortical and thalamic efferents J Comp Neurol 252:1–31.
Witter MP, Groenewegen HJ, Lopes de Silva FH, Lohman AHM. 1989a. Functional organization of the extrinsic and intrinsic circuitry of the parahippocampal region. Prog Neurobiol 33:161–253.
Witter MP, Van Hoesen GW, Amaral DG. 1989b. Topographical organization of the entorhinal projection to the dentate gyrus of the monkey. J Neurosci 9:216–228.
Witter MP, Naber PA, van Haeften T, Machielsen WC, Rombouts SA, Barkhof F, Scheltens P, Lopes da Silva FH. 2000. Cortico-hippocampal communication by way of parallel parahippocampal-subicular pathways. Hippocampus 10:398–410.
Young BJ, Otto T, Fox GD, Eichenbaum H. 1997. Memory representation within the parahippocampal region. J Neurosci 17:5183–5195.